Sensor-based control of nonholonomic mobile robots

Mauro Maya, Pascal Morin, Claude Samson

▶ **To cite this version:**

Sensor-based control of nonholonomic mobile robots

Mauro Maya-Mendez — Pascal Morin — Claude Samson

N° 5944

Juillet 2006

Thème NUM

Rapport de recherche

Sensor-based control of nonholonomic mobile robots

Mauro Maya-Mendez , Pascal Morin , Claude Samson

Abstract: The problem of tracking a moving target with a nonholonomic mobile robot, by using sensor-based control techniques, is addressed. Two control design methods, relying on the transverse function approach, are proposed. For the first method, sensory signals are used to calculate an estimate of the relative pose of the robot with respect to the target. This estimate is then used for the calculation of control laws expressed in Cartesian coordinates. An analysis of stability and robustness w.r.t. pose estimation errors is presented. The second method consists in designing the control law directly in the space of sensor signals. Both methods are simulated, with various choices of the control parameters, for a unicycle-type mobile robot equipped with a camera. Finally, experimental results are also reported.

Key-words: nonholonomic system, target tracking, sensor-based control, transverse function

Commande référencée capteur des robots non-holonomes

Résumé : Nous considérons le problème de suivi d'une cible mobile avec un robot mobile non-holonome, via des techniques de commande référencée capteurs. Deux méthodes de synthèse de lois de commande, basées sur l'approche par fonctions transverses, sont proposées. Pour la première méthode, les données capteurs sont d'abord utilisées pour la reconstruction d'une estimée de la pose du robot par rapport à la cible. Cette estimée est ensuite utilisée pour le calcul de boucles de commande exprimées en coordonnées cartésiennes. Une analyse de stabilité et de robustesse par rapport aux erreurs d'estimation de la pose du robot est proposée. La deuxième méthode consiste à synthétiser directement la loi de commande dans l'espace des signaux capteur. Les deux méthodes sont testées en simulation, avec divers choix des paramètres de commande, pour un véhicule de type unicycle equippé d'une caméra embarquée. Enfin, des résultats expérimentaux sont présentés.

Mots-clés : système non-holonome, suivi de cible, commande référencée capteur, fonction transverse

Contents

1   Introduction

Sensor-based control, which consists essentially in using exteroceptive measurements in feedback loops, is an important technique for robotic applications that require the positioning of the controlled robotic device with respect to (w.r.t.) some external object/target. It has first been developed for, and applied to, manipulator arms [13, 12, 5, 6] in order to perform tasks such as pick and place, welding, or pointing, by using the information about the surrounding environment provided by exteroceptive sensors. Many sensor-based applications have also emerged from the more recent development of mobile robotics. For example, visual servoing is used for path following, target tracking, or platooning tasks [11, 4]. The present study is devoted to the sensor-based control of nonholonomic mobile robots with a focus on robotic tasks which rely on the regulation of *both* the position and orientation of the robot, i.e., on the control of the complete posture of the mobile platform. An abundant literature has been devoted to the control of nonholonomic systems in order to tackle various challenging issues associated with the problem. Two of the authors of the present paper have worked on these questions for years and the reader is referred to [10] where these issues are surveyed in some detail. Among them, the problem of stabilizing state trajectories which are not necessarily feasible for the system has received little attention, whereas we believe that it is very relevant for a number of applications, an example of which is treated further. The fact that non-feasible trajectories cannot, by definition, be asymptotically stabilized, combined with other difficulties and impossibilities (see [10] and [7], for instance) related to Brockett's theorem [3] according to which asymptotic stabilization of a fixed point is not solvable by using smooth pure-state feedback, and also the common experience that infinite precision in the posture control of a mobile robot is seldom necessary in practice, suggests that, for nonholonomic systems, the classical objective of *asymptotic* stabilization of a desired (reference) state or trajectory is not best suited to qualify what can be achieved with feedback control. By contrast, the slightly weaker objective, considered in [8], of asymptotic stabilization of a set contained in an arbitrarily small neighborhood of the reference state allows to avoid all theoretical obstructions associated with the former objective. Its satisfaction guarantees, for instance, that the tracking error can be ultimately bounded by a pre-specified (non-zero) value, whether the reference trajectory is, or is not, feasible (provided only that it is smooth enough). The Transverse Function (TF) approach, the basics of which are described in [8], provides a way of designing smooth feedback laws which satisfy this objective. Experimental validations of this approach for the tracking of an omnidirectional target have been reported in [1, 2]. The present paper goes in the same direction, with the complementary preoccupation of studying the robustness of the control when the target is observed with sensors whose characteristics are either imperfectly modeled or purposefully simplified. Two control strategies are considered. The first one is based on a pose estimation (in the sense of e.g. [6]), and one of the contribution of the paper is the derivation of sufficient conditions upon the pose estimation method under which closed-loop stability is granted. In particular, we prove that a crude pose estimation obtained by using an estimate of the sensor's interaction matrix can yield good tracking precision. The second strategy consists in designing feedback

laws in the space of the sensor signals (i.e. without having to estimate the robot's pose). The analysis is illustrated and complemented by simulation and experimental results.

The paper is organized as follows. The studied control problem is presented in Section 2. Kinematic models and basic results about the application of the TF approach to the design of practical stabilizers are recalled in Section 3. Combining sensor-based pose estimation and control is addressed in Section 4, along with stability conditions for the resulting sensor-based controllers. Finally, the control design approach in the signal space is presented in Section 5.

2 Problem statement

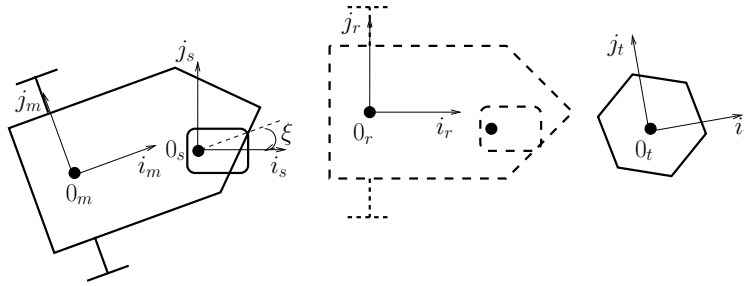Consider the setup depicted on Fig. 1. The non-holonomic mobile robot (on the left-side)

Figure 1: Mobile robot (l), reference situation (m), and target (r)

is equipped with a sensor (a camera, for instance) providing information about its relative situation w.r.t. a moving object, called the *target*. For simplicity, all bodies are represented by their projections on the robot's plane of motion. A frame $\mathcal{F}_m = \{0_m, \overrightarrow{i_m}, \overrightarrow{j_m}\}$ is attached to the mobile platform, and g_{om} denotes the situation of this frame w.r.t. some fixed frame $\mathcal{F}_0$. This is an element of the Special Euclidean group $SE(2)$, itself isomorphic to $\mathbb{R}^2 \times \mathbb{S}^1$. Another frame $\mathcal{F}_s = \{0_s, \overrightarrow{i_s}, \overrightarrow{j_s}\}$ is attached to the sensor, and g_{os} denotes the situation of this frame w.r.t. $\mathcal{F}_0$. The relative situation g_{ms} of the sensor w.r.t. the platform is parameterized by the pan angle ξ. The control of this angle can be performed on the basis of the simple kinematic model $\dot{\xi} = v_\xi$, with v_ξ the associated velocity control variable. The sensor delivers a vector-valued signal $s \in \mathbb{R}^3$ which only depends on the relative situation g_{ts} of the sensor frame w.r.t. a frame $\mathcal{F}_t = \{0_t, \overrightarrow{i_t}, \overrightarrow{j_t}\}$ attached to the target i.e. $s = \varphi(g_{ts})$. This implies the standard hypothesis that the target is rigid. It is assumed that g_{ts} is uniquely defined by s, at least within some operating domain. In fact, we will make the stronger assumption that φ is a diffeomorphism from an open domain of $SE(2)$ to an open domain of $\mathbb{R}^3$. The control objective is to stabilize the platform at a reference situation g_{or}, depicted in the middle of the figure, with the relative situation g_{tr} of the reference frame w.r.t. the target frame being predefined and constant. This is clearly equivalent to

stabilizing at zero the relative situation $g = g_{rm}$ between the frames $\mathcal{F}_m$ and $\mathcal{F}_r$. Note that maintaining this "tracking error" at zero permanently is obviously not possible in all cases, due to the nonholonomic constraint on the robot which forbids any instantaneous lateral motion. In fact, there are not many motions of the target for which this is possible. This is one of the reasons why practical stabilization, allowing for small tracking errors, is here preferred to the non-attainable classical objective of asymptotic stabilization which requires convergence of the error to zero.

3   Modeling and Preliminary recalls

3.1   Group operation in $SE(2)$ and parameterization

Since $SE(2)$ is a Lie group isomorphic to $\mathbb{R}^2 \times \mathbb{S}^1$, one can identify an element g of this group with a three-dimensional "vector" $(p', \theta)'$, with $p = (x, y)' \in \mathbb{R}^2$, $\theta \in \mathbb{S}^1$, and the prime superscript denoting the transpose operation. When using an element of this group, say $g_{om} = (p'_{om}, \theta_{om})'$, to characterize the situation of a frame, $\mathcal{F}_m$, with respect to another, $\mathcal{F}_o$, the vector p_{om} is the vector of coordinates of 0_m in the frame $\mathcal{F}_o$ and θ_{om} is the oriented angle between $\overrightarrow{\imath_o}$ and $\overrightarrow{\imath_m}$.

$SE(2)$ is endowed with the group operation defined by

$$(g_1, g_2) \longmapsto g_1 g_2 := \begin{pmatrix} p_1 + R(\theta_1)p_2 \\ \theta_1 + \theta_2 \end{pmatrix} \tag{1}$$

with $R(\theta)$ the rotation matrix of angle θ. The unit element e of this group (such that $ge = eg = g$) is $e = (0,0)$ and the inverse g^{-1} of g (such that $gg^{-1} = g^{-1}g = e$) is

$$g^{-1} = \begin{pmatrix} -R(-\theta)p \\ -\theta \end{pmatrix} \tag{2}$$

From now on, e will also be denoted as 0. It follows from these relations that the situation g_{ab} of a frame $\mathcal{F}_b$ w.r.t. a frame $\mathcal{F}_a$ satisfies the relation $g_{ab} = g_{oa}^{-1}g_{ob}$. Note also that $g_{ab} = g_{ba}^{-1}$ and $g_{ab}g_{ba} = 0$.

A distance between $g = (p', \theta)'$ and 0 is given[1] by $\|g\| = \sqrt{\|p\|^2 + \theta^2}$ with $\|p\|$ the Euclidean norm of the vector p, and θ identified with its representative in $(-\pi/2; \pi/2]$. Finally, we denote by $B_g(\delta)$ the "ball" in $SE(2)$ of radius δ and centered at 0, i.e. $B_g(\delta) = \{g \in SE(2) : \|g\| \leqslant \delta\}$.

3.2   Kinematic modeling

With $g_{om} = (x_{om}, y_{om}, \theta_{om})'$ denoting the situation of the robot's frame $\mathcal{F}_m$ (see Fig. 1) w.r.t. an inertial frame $\mathcal{F}_o$, the kinematic equations of the mobile platform are given by

$$\dot{g}_{om} = X(g_{om})C(\zeta)v \tag{3}$$

---

[1]with a slight abuse of notation because $SE(2)$ is not a vector space and thus cannot be endowed with a norm

with

$$X(g_{om}) = \begin{pmatrix} \cos\theta_{om} & -\sin\theta_{om} & 0 \\ \sin\theta_{om} & \cos\theta_{om} & 0 \\ 0 & 0 & 1 \end{pmatrix} \tag{4}$$

$C(\zeta)$ a matrix that may depend on the variable ζ of internal states (e.g., steering angles), and v a vector of instantaneous velocities. When the platform is omnidirectional, $C(\zeta)$ is simply the identity matrix and $dim(v) = 3$, v_1 and v_2 correspond to the components of the velocity vector of 0_m expressed in $\mathcal{F}_m$, and v_3 denotes the angular velocity of $\mathcal{F}_m$. When the mobile platform is of unicycle type, the velocity vector of 0_m is bound to be parallel to $\overrightarrow{i_m}$, so that

$$C(\zeta) = C = \begin{pmatrix} 1 & 0 \\ 0 & 0 \\ 0 & 1 \end{pmatrix} \tag{5}$$

and $dim(v) = 2$, v_1 corresponds to the velocity vector of 0_m expressed in $\mathcal{F}_m$, and v_2 denotes the angular velocity of $\mathcal{F}_m$. Eq. (3) then gives the well known equations

$$\begin{cases} \dot{x}_{om} &= v_1\cos\theta_{om} \\ \dot{y}_{om} &= v_1\sin\theta_{om} \\ \dot{\theta}_{om} &= v_2 \end{cases} \tag{6}$$

When the mobile platform is a car,

$$C(\zeta) = \begin{pmatrix} 1 \\ 0 \\ \delta \end{pmatrix} \tag{7}$$

with $\delta = (\tan\varphi)/\ell$, φ the steering angle, and ℓ the distance between the front wheels and rear wheels axes. In this case $dim(v) = 1$ i.e. $v = v_1$ is the velocity of 0_m expressed in $\mathcal{F}_m$. Equation (3) then gives

$$\begin{cases} \dot{x}_{om} &= v_1\cos\theta_{om} \\ \dot{y}_{om} &= v_1\sin\theta_{om} \\ \dot{\theta}_{om} &= v_1\delta = v_1(\tan\varphi)/\ell \end{cases} \tag{8}$$

Let us remark that the kinematic model of a car involves the complementary equation $\dot{\varphi} = v_2$ or, equivalently, (i.e. by a change of control variable), $\dot{\delta} = v_\delta = v_2/(\ell\cos^2\varphi)$.

A characteristic property of System (3) is its left-invariance w.r.t. the group operation on $SE(2)$. This property means that the system equations are the same whatever the inertial frame w.r.t. which they are expressed, i.e. $\dot{g}_{ap} = X(g_{ap})C(\zeta)v$ for any inertial frame $\mathcal{F}_a$. More generally, given any two smooth curves $g_1(.), g_2(.)$ with $\dot{g}_i = X(g_i)c_i$, we have the following relations (easily derived from (1)):

$$\begin{aligned} \tfrac{d}{dt}(g_1^{-1}g_2) = \tfrac{d}{dt}(g_{12}) &= X(g_{12})(c_2 - \mathrm{Ad}^X(g_{21})c_1) \\ \tfrac{d}{dt}(g_1g_2^{-1}) &= X(g_1g_2^{-1})\mathrm{Ad}^X(g_2)(c_1 - c_2) \end{aligned} \tag{9}$$

with

$$\text{Ad}^X(g) = \begin{pmatrix} R(\theta) & \begin{pmatrix} y \\ -x \end{pmatrix} \\ 0 & 1 \end{pmatrix} \tag{10}$$

the matrix associated with the adjoint operator at $g = (x, y, \theta)'$.

It follows from (3) and (9) that the relative situation $g := g_{or}^{-1} g_{om}$ $(= g_{rm})$ of the mobile platform's frame $\mathcal{F}_m$ w.r.t. the reference frame $\mathcal{F}_r$ satisfies the following equation:

$$\dot{g} = X(g) \left(C(\zeta)v - \text{Ad}^X(g^{-1})c_r(t) \right) \tag{11}$$

with $c_r(t)$ the reference frame's velocity vector (at time t) defined by

$$\dot{g}_r(t) = X(g_r)c_r(t)$$

Important: From now on, to simplify the notation, g will always stand for g_{rm}.

The relative situation g can be viewed as a "tracking error" that the control v is in charge of stabilizing at zero. Relation (11) points out that it is not possible to keep this error equal to zero when the reference trajectory is not feasible for the nonholonomic platform, like for example when the second component of $c_r(t)$ is different from zero. We recall in the next section the design of *practical* stabilizers based on the TF approach.

3.3 Practical stabilization based on the transverse function approach

The transverse function (t.f.) approach [8] provides a general framework for the practical stabilization of nonholonomic systems. We recall hereafter some elements of this approach for systems modeled[2] by (3), and refer the reader to [8] for more details and complementary results.

Definition 1 *A smooth function $f = (f_g', f_\zeta')'$ defined on the p-dimensional torus $\mathbb{T}^p$ (with $\mathbb{T} = \mathbb{R}/2\pi\mathbb{Z}$) is called a* transverse function *for System (3) if, for any $\alpha \in \mathbb{T}^p$, the matrix*

$$\begin{pmatrix} X(f_g(\alpha))C(f_\zeta(\alpha)) & \dfrac{\partial f_g}{\partial \alpha}(\alpha) \end{pmatrix} \tag{12}$$

is of rang three $(= \dim(SE(2)))$.

Remark 1 *Since $X(g)$ is an invertible matrix for any g, there exists a matrix $A(\alpha)$ such that $\frac{\partial f_g}{\partial \alpha}(\alpha) = X(f_g(\alpha))A(\alpha)$. With this notation, the matrix (12) is of rank three if and only if the matrix*

$$\bar{C}(\alpha) = (C(f_\zeta(\alpha)) \quad - A(\alpha)) \tag{13}$$

is also of rank three.

---

[2]We implicitly assume here that the variable ζ, when it exists, can be viewed as a control variable; note that this is essentially the case for a car-like vehicle since $\dot{\delta}$ is directly controlled by the steering velocity.

Example (unicycle): Consider the function $f = f_g = (f_x, f_y, f_\theta)'$ defined on $\mathbb{T}$ by

$$f(\alpha) \quad = \quad \begin{pmatrix} \varepsilon \sin \alpha \\ \frac{\varepsilon^2}{4} \eta \sin 2\alpha \\ \arctan(\varepsilon \eta \cos \alpha) \end{pmatrix} \tag{14}$$

From (6) and Definition 1, f is a transverse function for the unicycle kinematic model if the matrix

$$\begin{pmatrix} \cos f_\theta(\alpha) & 0 & \frac{\partial f_x}{\partial \alpha}(\alpha) \\ \sin f_\theta(\alpha) & 0 & \frac{\partial f_y}{\partial \alpha}(\alpha) \\ 0 & 1 & \frac{\partial f_\theta}{\partial \alpha}(\alpha) \end{pmatrix}$$

is invertible for any α. One easily verifies that this condition is satisfied with the function f defined by (14) for any $\varepsilon, \eta > 0$.

Example (car): [10] Consider now the function $f = (f_g', f_\zeta)' = (f_x, f_y, f_\theta, f_\delta)'$ defined on $\mathbb{T}^2$ by

$$f(\alpha) = \left(\bar{f}_1(\alpha), \bar{f}_4(\alpha), \arctan(\bar{f}_3(\alpha)), \bar{f}_2(\alpha) \cos^3(f_\theta(\alpha)) \right)' \tag{15}$$

with

$$\bar{f}(\alpha) = \begin{pmatrix} \varepsilon(\sin \alpha_1 + \eta_2 \sin \alpha_2) \\ \varepsilon \eta_1 \cos \alpha_1 \\ \varepsilon^2 \left(\eta_1 \frac{\sin 2\alpha_1}{4} - \eta_3 \cos \alpha_2 \right) \\ \varepsilon^3 \left(\eta_1 \frac{\sin^2 \alpha_1 \cos \alpha_1}{6} - \eta_2 \eta_3 \frac{\sin 2\alpha_2}{4} - \eta_3 \sin \alpha_1 \cos \alpha_2 \right) \end{pmatrix}$$

From (8) and Definition 1, f is a transverse function for the car kinematic model if the matrix

$$\begin{pmatrix} \cos f_\theta(\alpha) & \frac{\partial f_x}{\partial \alpha_1}(\alpha) & \frac{\partial f_x}{\partial \alpha_2}(\alpha) \\ \sin f_\theta(\alpha) & \frac{\partial f_y}{\partial \alpha_1}(\alpha) & \frac{\partial f_y}{\partial \alpha_2}(\alpha) \\ f_\delta(\alpha) & \frac{\partial f_\theta}{\partial \alpha_1}(\alpha) & \frac{\partial f_\theta}{\partial \alpha_2}(\alpha) \end{pmatrix}$$

is invertible for any $\alpha = (\alpha_1, \alpha_2)$. One can verify that this condition is satisfied with the function f defined by (15) for any $\varepsilon > 0$, and any $\eta_1, \eta_2, \eta_3 > 0$ such that $6\eta_2\eta_3 > 8\eta_3 + \eta_1\eta_2$.

The following result shows that the knowledge of a transverse function allows to design feedback laws that guarantee *a)* the convergence of the tracking error g to a neighborhood of the origin, and *b)* the convergence of g to a fixed value when $c_r = 0$ (i.e. when the reference trajectory is fixed).

Proposition 1 *Let $f = (f_g', f_\zeta')'$ denote a transverse function for System (3), and let $\zeta = f_\zeta(\alpha)$ and $z = g f_g(\alpha)^{-1}$. Then,*

i) Along the solutions of the tracking error model (11), and for any smooth curve $\alpha(.)$,

$$\dot{z} = X(z) \mathrm{Ad}^X(f_g(\alpha)) \left(\bar{C}(\alpha)\bar{v} - \mathrm{Ad}^X(g^{-1}) c_r(t) \right) \tag{16}$$

with $\bar{v} = (v', \dot{\alpha}')'$ and $\bar{C}(\alpha)$ defined by (13).

ii) *The matrix $\bar{C}(\alpha)$ being of rank three for any α, the change of variable*

$$\bar{v} = \bar{C}(\alpha)^{\dagger} \left(\mathrm{Ad}^X(f_g(\alpha)^{-1})v_z + \mathrm{Ad}^X(g^{-1})c_r(t) \right) \tag{17}$$

with $\bar{C}(\alpha)^{\dagger}$ a right-inverse of $\bar{C}(\alpha)$, transforms System (16) into $\dot{z} = X(z)v_z$.

iii) *For any Hurwitz-stable matrix K, and for v_z defined by*

$$v_z = X(z)^{-1}Kz \tag{18}$$

    a) *$\|g\|$ is ultimately bounded by $\varepsilon_f := \max_{\alpha} \|f_g(\alpha)\|$ for any reference trajectory $g_r(.)$,*

    b) *if $c_r = 0$, g and g_{om} exponentially tend to fixed points in $SE(2)$.*

Property *i)* is a consequence of (9), (11), and (13). Property *ii)* directly follows from *i)*. Property *iii.a)* is easily deduced from the (exponential) convergence of z to zero. Property *iii.b)* also follows from this convergence property. Indeed, when $c_r = 0$, $\bar{v}$ tends to zero exponentially, so that g, and g_{om} are bound to converge to fixed values.

    Note that, with this approach, the derivative $\dot{\alpha}$ of the vector of variables (reduced to a scalar variable in the case of the example (14)) on which the transverse function depends plays the role of a complementary control vector.

4   Combined pose estimation and control

In order to implement the control (17)-(18) in Prop. 1, g has to be known at each time. In practice however, this information is often only available via the measurement provided by exteroceptive sensors embarked on the robot. Moreover, it is not completely accurate due to well known reasons such as imperfect modeling and calibration of the sensors. We now examine how the replacement, in the control expression, of g by a *pose estimate* $\hat{g}$ calculated from the sensory signal s modifies the above result.

4.1   Some techniques for pose estimation

Let us first recall that $s = \varphi(g_{ts})$ and that we have assumed that φ is a (local) diffeomorphism, so that φ^{-1} is also well defined locally. By the group law, one has $g = g_{rt}g_{ts}g_{sm}$, so that one can also write

$$g = g_{rt}\varphi^{-1}(s)g_{sm} \tag{19}$$

The calculation of an estimate $\hat{g}$ of g from sensory measurements corresponds to the classical "pose estimation problem", which has been widely studied in the robotics literature. Let us (without any claim of originality) briefly recall a few possible approaches. For example, it follows from (19) that

$$s = \varphi_s(g, \xi) := \varphi(g_{tr}gg_{ms}) \tag{20}$$

since g_{tr} is constant and $g_{ms} = g_{ms}(\xi)$. With s chosen so that $\varphi_s(0,0) = 0$, a simple linear estimate can be obtained from the local approximation $s \approx \frac{\partial \varphi_s}{\partial g}(0,0)g + \frac{\partial \varphi_s}{\partial \xi}(0,0)\xi$, i.e.

$$\hat{g} = \left(\widehat{\frac{\partial \varphi_s}{\partial g}}(0,0) \right)^{-1} \left(s - \widehat{\frac{\partial \varphi_s}{\partial \xi}}(0,0)\xi \right) \tag{21}$$

with $\widehat{\frac{\partial \varphi_s}{\partial g}}(0,0)$ and $\widehat{\frac{\partial \varphi_s}{\partial \xi}}(0,0)$ some approximations of $\frac{\partial \varphi_s}{\partial g}(0,0)$ and $\frac{\partial \varphi_s}{\partial \xi}(0,0)$. When the situation g_{ms} of the sensor w.r.t. the platform is known, and a model of φ is available, Eq. (19) can be used to derive nonlinear estimates. However, it is often difficult in practice to have a very accurate model of φ. Furthermore, what is in fact needed for the calculation of g is φ^{-1}, the inverse of φ. Having an analytical expression of φ does not imply that an analytical expression of φ^{-1} is available. When it is not, one can compute an estimate of $\varphi^{-1}(s)$ via a gradient search algorithm based on the use of the Jacobian matrix $\frac{\partial \varphi}{\partial g_{ts}}$. Another possibility consists in determining a function $\hat{\varphi}$ which approximates φ in some domain containing the desired situation $g_{ts}^* = \varphi^{-1}(0)$, and the inverse of which has an analytical expression. This yields the estimate

$$\hat{g} = g_{rt}\hat{\varphi}^{-1}(s)g_{sm} \tag{22}$$

Finally, even when an analytical expression of φ^{-1} is known, one may use a simplified expression for this function, in order to reduce the calculation load. This yields an estimate of g of the form

$$\hat{g} = g_{rt}\widehat{\varphi^{-1}}(s)g_{sm} \tag{23}$$

4.2 Sufficient conditions for ultimate boundedness and convergence

Now, let $\hat{z} := \hat{g}f_g(\alpha)^{-1}$. Using $\hat{z}$ instead of z in the feedback law (17)-(18) yields the following control:

$$\bar{v} = \bar{C}(\alpha)^{\dagger} \left(\mathrm{Ad}^X(f_g(\alpha)^{-1})X(\hat{z})^{-1}K\hat{z} + \mathrm{Ad}^X(\hat{g}^{-1})c_r(t) \right) \tag{24}$$

which can be simplified to

$$\bar{v} = \bar{C}(\alpha)^{\dagger}\mathrm{Ad}^X(f_g(\alpha)^{-1})X(\hat{z})^{-1}K\hat{z} \tag{25}$$

when c_r is equal to zero, or is unknown. The question is now to determine the properties of this control in terms of stability and convergence. To this purpose, we assume that $\hat{g}$ depends only on g, i.e. $\hat{g} = \psi(g)$. This is a natural assumption when the sensor is rigidly attached to the platform (i.e. $\xi \equiv 0$), since s only depends on g in this case. The extension to the case where ξ is actively controlled will be discussed and illustrated through application examples in the subsequent sections. Besides the requirement of $\hat{g}$ being a function of g, the following assumption is also made.

Assumption 1 *There exist some constants $\delta_1 > 0$ and $\gamma_1 < 1$ such that the estimation error $\tilde{g} = g\hat{g}^{-1}$ satisfies the inequality*

$$\|\tilde{g}\| \leqslant \gamma_1 \|g\|, \quad \forall g \in B_g(\delta_1) \tag{26}$$

Condition (26) means that the relative norm of the estimation error is less than one in some bounded domain containing $g = 0$. This is clearly a weak requirement. Indeed, since $\hat{g} = \psi(g)$ then, provided that $\psi(0) = 0$ (unbiased estimation at the desired location), one shows from the group law definition (1) that

$$\tilde{g} \approx \left(I_3 - \frac{\partial \psi}{\partial g}(0)\right) g \tag{27}$$

in the neighborhood of $g = 0$. Therefore, if $\|I_3 - \frac{\partial \psi}{\partial g}(0)\| < 1$, Assumption 1 is satisfied in some neighborhood of $g = 0$. For example, when $\hat{g}$ is defined according to (21) (with $\xi \equiv 0$), this relation becomes

$$\left\| I_3 - \left(\widehat{\frac{\partial \varphi_s}{\partial g}}(0)\right)^{-1} \frac{\partial \varphi_s}{\partial g}(0) \right\| < 1$$

This latter relation is reminiscent of a classical requirement upon the interaction matrix made in the context of sensor-based control of manipulator arms.

The following result, the proof of which is given in the appendix, establishes the ultimate boundedness of the tracking error g (compare with Property *iii.a)* in Proposition 1).

Proposition 2 *Consider the feedback law (25) with $K = -kI_3$ ($k > 0$) and f a transverse function. If*

$$\|g(0)\| < \delta_1 - 2\varepsilon_f \quad \text{and} \quad \bar{\varepsilon}_f := \frac{\varepsilon_f + \|c_r\|_{\max}/k}{1 - \gamma_1} < \delta_1 \tag{28}$$

with δ_1 and γ_1 some constants specified by (26) and $\|c_r\|_{\max} := \max_t \|c_r(t)\|$, then $\|g\|$ is ultimately bounded by $\bar{\varepsilon}_f$.

Let us make some comments on this result. First, the choice of the gain matrix K in the proposition is essentially made in order to simplify the proof and specify an ultimate bound for $\|g\|$. The ultimate boundedness is also guaranteed for other Hurwitz stable matrices, like e.g. any matrix of the form

$$K = \begin{pmatrix} -K_p & 0 \\ 0 & -k_\theta \end{pmatrix}$$

with K_p a 2×2 definite positive matrix and $k_\theta > 0$. Then, Condition (28) indicates how the "size" of the transverse function f influences the ultimate bound of g and the set of initial conditions $g(0)$ for which the boundedness can be proven. Finally, let us insist on the contribution of the present result: it points out that for *any* estimation $\hat{g}$ of g satisfying (26), the tracking error with respect to *any* reference trajectory is ultimately bounded by a

value that can be made arbitrarily small by a proper choice of the control parameters ε and k.

When the reference velocity is known, the feedback law (24) can be used to improve the tracking precision, as shown by the following proposition.

Proposition 3 *Assume that the reference's velocity $c_r(t)$ is known and consider the dynamic feedback law (24) with $K = -kI_3$ $(k > 0)$ and f a transverse function. If*

$$\|g(0)\| < \delta_1 - 2\varepsilon_f \quad \text{and} \quad \bar{\varepsilon}_f := \frac{\varepsilon_f}{1 - \gamma_1(1 + \|c_r\|_{\max}/k)} < \delta_1$$

with δ_1 and γ_1 some constants specified by (26) and $\|c_r\|_{\max} := \max_t \|c_r(t)\|$, then $\|g\|$ is ultimately bounded by $\bar{\varepsilon}_f$.

The proof of this result, similar to the proof of Proposition 2, is left to the reader.

We now address the issue of convergence to a fixed situation when the target is motionless (compare with Property *iii.b)* in Proposition 1). In contrast with the above propositions, the cases of unicycle-like and car-like platforms must be treated separately.

Proposition 4 *For the unicycle model (6), consider the feedback law (25) with $K = -kI_3$ $(k > 0)$, and f a transverse function defined by (14). Assume that $c_r = 0$ (i.e., the target is fixed), and that Condition (28) is satisfied. Let γ_2 denote the smallest constant such that*

$$\left\|\frac{\partial \psi}{\partial g}(g) - \frac{\partial \psi}{\partial g}(0)\right\| \leqslant \gamma_2 \|g\|, \quad \forall g \in B_g(\varepsilon_f/(1 - \gamma_1)) \tag{29}$$

There exist two positive numbers c_1 and c_2, which only depend on the parameter η of the transverse function f, such that if

$$\bar{\gamma} := \left(\gamma_1 + (\gamma_1 + \gamma_2)\frac{\varepsilon_f}{1 - \gamma_1}\right)\left(\frac{c_1}{\varepsilon_f} + c_2\varepsilon_f^3\right) < 1 \tag{30}$$

then $\hat{z}$ exponentially converges to zero and g exponentially converges to a fixed value.

With respect to Proposition 2, the above result involves the additional condition (30). Let us discuss how the "size" ε_f of the transverse function (which is essentially given by the parameter ε), and the values of γ_1, γ_2 (which reflect the quality of the pose estimation) influence the satisfaction of this condition. For $\varepsilon_f \in [0, \bar{\varepsilon}]$, condition (30) is satisfied if

$$\left(\gamma_1 + (\gamma_1 + \gamma_2)\frac{\varepsilon_f}{1 - \gamma_1}\right)\frac{\bar{c}_1}{\varepsilon_f} < 1 \tag{31}$$

with $\bar{c}_1 = c_1 + c_2\bar{\varepsilon}^4$. It is clear that this condition cannot be satisfied, when ε_f tends to zero, unless $\gamma_1 = 0$. This suggests that very small values of ε_f, yielding very precise tracking, may not allow the robot to converge to a resting situation when the target is motionless. This

is consistent with the difficulty of achieving both exponential stability of a fixed situation and robustness of this property w.r.t. modeling errors in the case of nonholonomic vehicles (see [10] for more details). Nevertheless, the condition (30) shows also that, for any value of ε_f, exponential convergence occurs if γ_1 and γ_2 are small enough. It follows from (27) that γ_1 is small in the neighborhood of $g = 0$ if the Jacobian of ψ at this point is close to the identity. For example, when $\hat{g}$ is given by (21), this condition is satisfied if the Jacobian of the function φ_s is accurately estimated. In this case, if one assumes, to simplify, that $\gamma_1 = 0$, then condition (31) simplifies to $\gamma_2 \bar{c}_1 < 1$. The constant $\bar{c}_1$ can be calculated from the parameters of the transverse function. As for γ_2, it is directly related to second order terms of the function ψ and, thus, to second order terms of the signal function φ_s. For this reason, unless an analytic model of φ_s is known, it is usually difficult to evaluate γ_2. Let us note, however, that $\gamma_2 = 0$ when ψ is a linear mapping. Finally, let us remark that (30) is only a *sufficient* condition for convergence. Simulation and experimental results, like those presented in the next sections, tend to indicate that it is quite conservative. In fact, extensive simulations with various choices of the signal function did not allow us to observe situations for which the tracking error remained bounded but did not converge to a fixed value. Whether this property is, or is not, always satisfied thus remains an open question.

For car-like platforms, one obtains the following result similar to Proposition 4, with (30) replaced by a more restrictive condition.

Proposition 5 *For the car model* (8), *consider the feedback law* (25) *with* $K = -kI_3$ ($k > 0$), *and* f *a transverse function defined by* (15). *Assume that* $c_r = 0$, *and that Condition* (28) *is satisfied. Let* γ_2 *denote the smallest constant such that*

$$\left\| \frac{\partial \psi}{\partial g}(g) - \frac{\partial \psi}{\partial g}(0) \right\| \leqslant \gamma_2 \|g\|, \quad \forall g \in \mathrm{B_g}(\varepsilon_f/(1 - \gamma_1)) \tag{32}$$

There exist two positive numbers c_1 *and* c_2, *which only depend on the parameters* η_i *of the transverse function* f, *such that if*

$$\bar{\gamma} := \left(\gamma_1 + (\gamma_1 + \gamma_2) \frac{\varepsilon_f}{1 - \gamma_1} \right) \left(\frac{c_1}{\varepsilon_f^2} + c_2 \varepsilon_f^4 \right) < 1 \tag{33}$$

then $\hat{z}$ *exponentially converges to zero and* g *exponentially converges to a fixed value.*

The proof of this proposition, which is much alike the proof of Proposition 4 is also given in the appendix. The main difference comes from the term $1/\varepsilon_f^2$ in (33), due to the fact that the third component of the transverse function (15) is homogeneous to ε^2, whereas the third component of the transverse function (14) associated with the unicycle is homogeneous to ε. Apart from this, the conclusions which can be drawn out from Proposition 5 are qualitatively the same as for Proposition 4.

4.3 Simulation results for a vision-based sensor

The simulation results presented below have been obtained with the system depicted on Fig. 2, composed of a unicycle-like robot equipped with a pan video camera. The target is materialized by three non-collinear points, labeled as L, M, and R, which are the vertices of an isosceles triangle of base $2a$ and height b, with $a = b = 0.25$. The sensor signal is $s = (\mathbf{l} - \mathbf{l^*}, \mathbf{m} - \mathbf{m^*}, \mathbf{r} - \mathbf{r^*})'$, with $\mathbf{l}, \mathbf{m}, \mathbf{r}$ denoting the y-coordinates (in the camera frame) of the projection of the points L, M, R on the image plane, and $\mathbf{x^*}$ the value of the variable $\mathbf{x}$ at the reference position. For all simulations, $g_{tr} = (-2.5, 0, 0)'$ (this corresponds to the platform being aligned with the target at the reference situation, as shown on the figure), and $g_{ms} = (0.51, 0, \xi)'$.
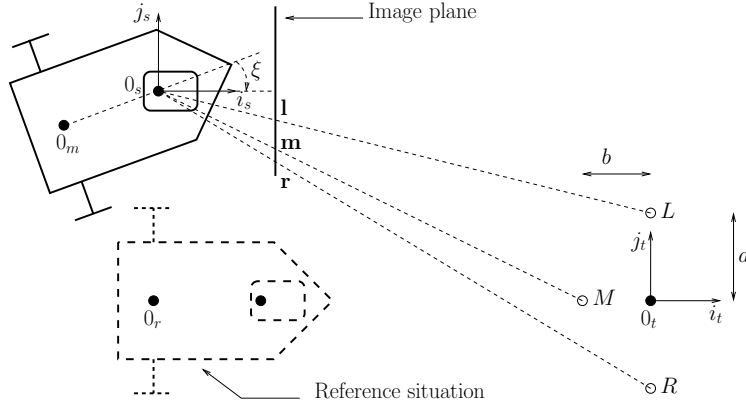

Figure 2: Unicycle-like robot with a vision-based sensor

4.3.1 Linear pose estimation

We first illustrate the use of the simple linear pose estimate defined by (21). This model requires to estimate the Jacobian matrices $\frac{\partial \varphi_s}{\partial g}(0,0)$ and $\frac{\partial \varphi_s}{\partial \xi}(0,0)$. This can be done by generating small displacements $\Delta g(p), \Delta \xi(p)$ $(p = 1, \ldots, P)$ in the neighborhood of $g = 0$ and $\xi = 0$, measuring the associated signal variations $\Delta s(p)$, and setting for instance (among other possibilities)

$$\left(\widehat{\frac{\partial \varphi_s}{\partial g}}(0,0) \; \widehat{\frac{\partial \varphi_s}{\partial \xi}}(0,0) \right) = (\Delta s(1) \cdots \Delta s(P)) \left(\begin{array}{c} \Delta g(1) \cdots \Delta g(P) \\ \Delta \xi(1) \cdots \Delta \xi(P) \end{array} \right)^{\dagger}$$

Fixed camera pan angle We first consider the case when $\xi = 0$. Then both s and $\hat{g}$ depend on g solely, so that the analysis of Section 4.2 applies directly. The simulation results reported on Fig. 3 have been obtained with a fixed target. The norms of g and $\hat{z}$
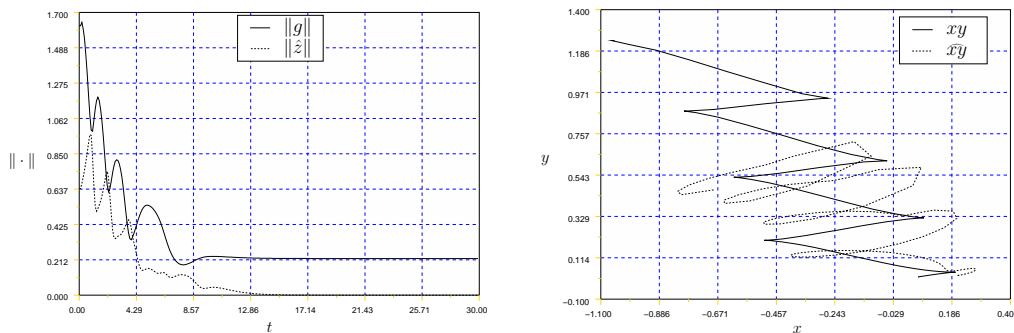
Figure 3: Linear estimation of g, no pan-control of the camera, fixed target

are displayed on the top sub-figure, and the bottom sub-figure corresponds to the motion of the origin 0_m of the robot's frame in the plane. The actual motion is drawn in plain lines whereas the motion deduced from the pose estimate (21) is drawn in dashed lines. The control law (25) has been applied with $K = -0.5I_3$, and the transverse function defined by (14) for $\varepsilon = 0.3$ and $\eta = 1$. The robot starts from the initial condition $g(0) = (-1.05, 1.24, 0)'$ (upper-left corner of the right sub-figure) and the final position is approximately given by $g(30) = (0.07, -0.03, 0.24)'$. Despite the poor quality of the estimation of g when the robot is far from the desired location, the controlled variable $\hat{z}$ converges to zero and the platform converges to a fixed situation near the desired one.

Active control of the camera pan angle In practice, it is often necessary to control the pan angle ξ so that the target remains inside the field of view of the camera. A simple control strategy consists in choosing v_ξ $(= \dot{\xi})$ in order to stabilize s_2 to zero (see Fig. 2). To this purpose, a simple proportional feedback, with precompensation of the mobile platform's rotation, in the form

$$v_\xi = k_s s_2 - v_2 \quad (k_s > 0) \tag{34}$$

will usually suffice. Using a relatively large value of the gain k_s helps to reduce the drag resulting from the uncompensated motion of the target. One could also derive more sophisticated control laws in order to better stabilize s_2 to zero in all situations, but this is not necessary since the objective, at this level, is only to maintain the target in the field of view of the camera.

Fig. 4 illustrates this strategy. The control law (25) has been applied with the same gain matrix K and transverse function as in the previous simulation, and with the control v_ξ defined by (34) for $k_s = 3$ and s expressed in metric coordinates. While the estimation of the platform's situation is significantly different from the one obtained for the previous simulation, the actual platform's motion is not much different qualitatively.
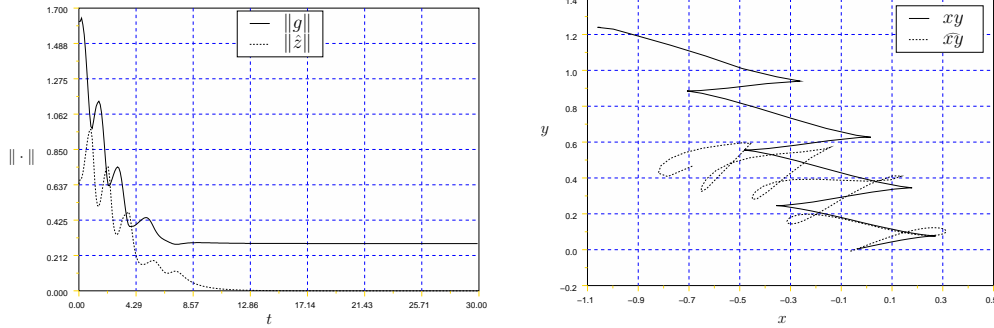
Figure 4: Linear estimation of g, pan-control of the camera, fixed target

The same control strategy is illustrated on Fig. 5 in the case of a moving target. The reference velocity c_r is defined as follows:

$$c_r(t) = \begin{cases} (0,0,0)' & \forall t \in [0,15) \\ (0.2,0,0)' & \forall t \in [15,30) \\ (0,0.2,0)' & \forall t \in [30,45) \\ (-0.2,0,0)' & \forall t \in [45,60) \\ (0,0,0.2)' & \forall t \in [60,75) \\ (0,0,0)' & \forall t \in [75,90] \end{cases} \tag{35}$$

The motions of the robot (plain lines) and reference frame (dashed lines) are shown on the right sub-figure. One can observe that the robot executes many manœuvres when $t \in [30,45)$. This is related to the fact that the reference trajectory is not feasible on this time-interval since $c_{r,2} \neq 0$. As in the case of the two previous simulations, many manœuvres are also executed in the initial phase, when the target is fixed and the robot is still far from the target (i.e., $t \in [0,15]$). The number of these manœuvres can be significantly reduced, for example by planifying a reference trajectory from the initial robot's pose to the desired pose, or by using a nonlinear gain scheduling such as the one proposed in [2]. Due to the non-measurement of the target's velocity (on which $c_r(t)$ depends), the tracking error increases when $c_r(t) \neq 0$ (as shown on the left sub-figure). The use of feedforward control, when c_r is known or can be accurately measured/estimated, improves this point significantly. One can also observe small oscillations of the robot's motion when the target moves along a straight line in the direction of $-\vec{\imath}_t$ (i.e., on the time-interval $[45,60]$). This phenomenon is a consequence of the non-perfect estimation of the robot's pose, since it does not occur when $\hat{g} = g$. It tends to occur for backward motions of the target (i.e., in the direction of $-\vec{\imath}_t$), as a consequence of the reduced distance between the robot and the target, and the fact that the estimation error increases rapidly when the distance between the camera and the target becomes small. However, we will see that such oscillations can also occur when the target moves forward in the direction of $\vec{\imath}_t$.
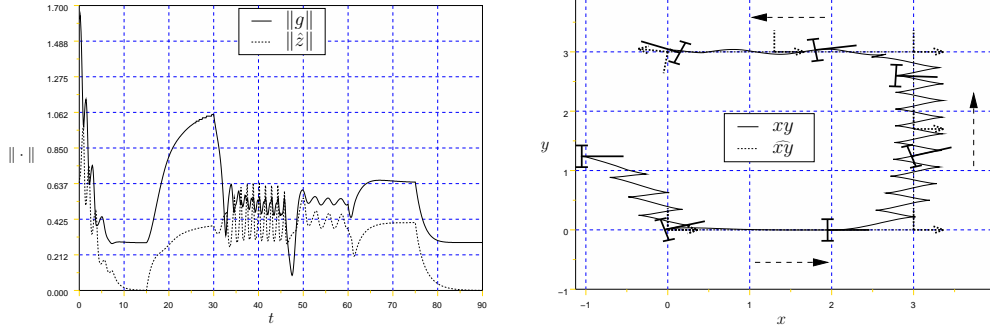
Figure 5: Linear estimation of g, pan-control of the camera, $\hat{c}_r = 0$
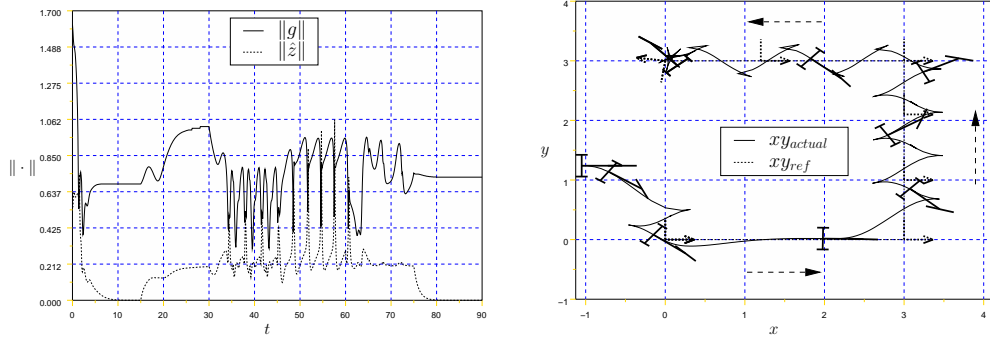
Figure 6: Car: Linear estimation of g, pan-control of the camera, $\hat{c}_r = 0$

Car   Figure 6 illustrates the same control strategy for a car-like vehicle. The linear estimation $\hat{g}$ of g used for the previous simulation is also utilized, and c_r is again defined by (35). The camera pan-control is also given by (34) with $k_s = 3$. The transverse function is defined by (15) with $\varepsilon = 0.17$, $\eta_1 = 15$, $\eta_2 = 1.7$, $\eta_3 = 30$. The control law $\bar{v}$, from which the velocity v_1 of Model (8) can be deduced, is given by (25) with $K = I_3$. The variable δ is set equal to $f_\delta(\alpha)$, with the asymptotic stabilization of $\delta - f_\delta(\alpha) = 0$ being granted by setting $v_\delta = \dot{f}_\delta(\alpha) - k(\delta - f_\delta(\alpha))$ with $k > 0$. The motions of the robot (plain lines) and reference frame (dashed lines) are shown on the right sub-figure. One can essentially draw the same conclusions as for the previous simulations. The fact that the number of maneuvers is smaller than for the previous simulation is only due to the choice of the transverse functions parameters (which are relatively large in the present case). However, one can observe that the oscillation phenomenon, when the target moves backward, is much stronger. The reasons of this amplification have not yet been elucidated.

4.3.2 Nonlinear pose estimation

When an analytical model of the sensor's output function φ (or of its inverse φ^{-1}) is known, the number of possibilities for the robot's pose estimation increases significantly. We illustrate below, in the case of our vision-based sensor, some possibilities associated with the expressions (22) and (23) of the estimate $\hat{g}$.

Estimation of g from an approximation of φ and inversion of $\hat{\varphi}$ (Eq. (22)): Let us assume that $\mathbf{l}, \mathbf{m}, \mathbf{r}$ are expressed in metric coordinates. From the target's geometry (cf. Fig. 2), we deduce that

$$\mathbf{l} = f\frac{y_{st} + a\cos\theta_{st}}{x_{st} - a\sin\theta_{st}}, \quad \mathbf{m} = f\frac{y_{st} - b\sin\theta_{st}}{x_{st} - b\cos\theta_{st}}, \quad \mathbf{r} = f\frac{y_{st} - a\cos\theta_{st}}{x_{st} + a\sin\theta_{st}} \tag{36}$$

with f the focal distance. Note that these relations define the function φ (once $x_{st}, y_{st}, \theta_{st}$ have been replaced by their expressions in terms of x_{ts}, y_{ts}, and θ_{ts}). The fact that $\theta_{st} = 0$ at the desired reference situation suggests approximating $\sin\theta_{st}$ by θ_{st}, and $\cos\theta_{st}$ by one, in the above equalities. This yields the following expression of $\hat{\varphi}$:

$$\hat{s} = \hat{\varphi}(g_{ts}) = \left(f\frac{y_{st} + a}{x_{st} - a\theta_{st}}, f\frac{y_{st} - b\theta_{st}}{x_{st} - b}, f\frac{y_{st} - a}{x_{st} + a\theta_{st}} \right)' \tag{37}$$

Once again, x_{st}, y_{st}, and θ_{st}, in the above equation should be replaced by their expressions in terms of x_{ts}, y_{ts}, and θ_{ts}, in order to obtain the analytical expression of $\hat{\varphi}$. Eq. (37) yields the following estimation of g_{st}, given s:

$$\hat{g}_{st} = \begin{pmatrix} \hat{x}_{st} \\ \hat{y}_{st} \\ \hat{\theta}_{st} \end{pmatrix} = P^{-1}q \quad \text{with } P := \begin{pmatrix} \mathbf{l} & -f & -a\mathbf{l} \\ \mathbf{r} & -f & a\mathbf{r} \\ \mathbf{m} & -f & bf \end{pmatrix} \quad \text{and } q := \begin{pmatrix} af \\ -af \\ \mathbf{m}b \end{pmatrix} \tag{38}$$

and the approximation $\hat{\varphi}^{-1}(s)$ of $\varphi^{-1}(s)$:

$$\hat{\varphi}^{-1}(s) := \hat{g}_{ts} := \hat{g}_{st}^{-1}$$

with $\hat{g}_{st}^{-1}$ the inverse of $\hat{g}_{st}$ w.r.t. the Lie group operation on $SE(2)$ (cf Eq. (2)). The estimate $\hat{g}$ is then calculated according to (22). Figures 7 and 8 illustrate this strategy for a fixed target and a moving target respectively. Except for the choice of the estimate $\hat{g}$, all the control parameters are the same as those used for the simulations of Fig. 4 and 5. As expected, one can observe from Fig. 4 and 7 that, in comparison with the linear approximation considered before, the nonlinear solution provides a much better estimate, especially when $\|g\|$ is large. While this has little influence on the robot's motion when the target is fixed, the quality of the estimation contributes to improving the tracking precision when the target moves (compare the left parts of Fig. 8 and 5), and to the suppression of the oscillation phenomenon when the target moves backward (compare the right parts of Fig. 8 and 5).
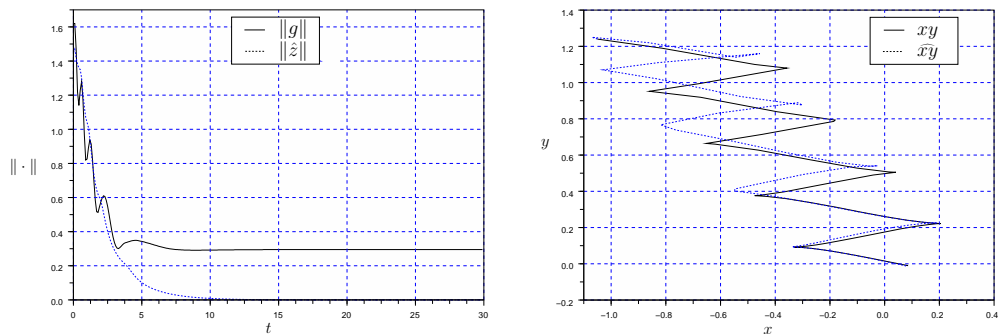
Figure 7: Nonlinear estimation of g: estimation of φ and inversion of $\hat{\varphi}$, pan-control
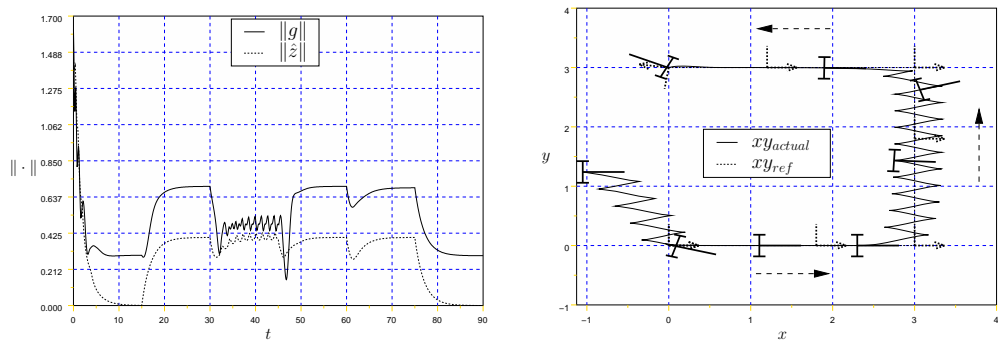
Figure 8: Nonlinear estimation of g: estimation of φ and inversion of $\hat{\varphi}$, pan-control, $\hat{c}_r = 0$
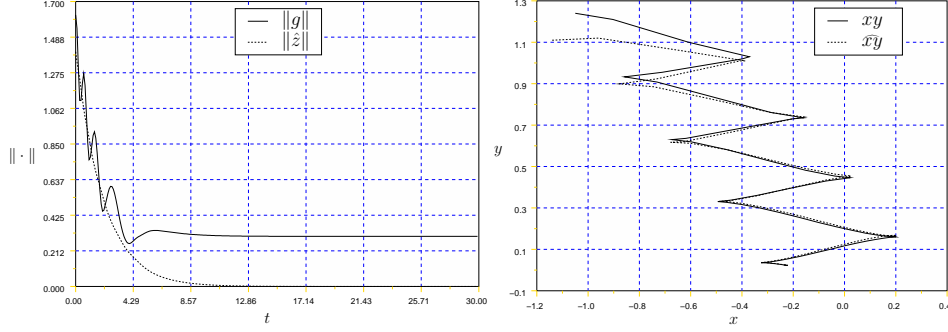
Figure 9: Nonlinear estimation of g: approximation of φ^{-1}, pan control

Estimation of g from an approximation of φ^{-1} (Eq. (23)): We now propose to directly approximate the pose $g_{ts} = \varphi^{-1}(s)$ from the sensor data s. A geometrical method to determine the function φ^{-1} is presented in the appendix. It yields the following equalities:

$$\begin{cases} x_{ts} &= -a\frac{|f+\mathbf{lr}/f|}{1-\mathbf{r}} - r_{rl}\cos\sigma \\ y_{ts} &= -r_{rl}\sin\sigma \\ \theta_{ts} &= \arctan\left(\frac{y_{ts}}{x_{ts}+b}\right) - \arctan\left(\frac{\mathbf{m}}{f}\right) \end{cases} \tag{39}$$

with

$$r_{rl} = \frac{a\sqrt{(f+\frac{\mathbf{lr}}{f})^2 + (\mathbf{l}-\mathbf{r})^2}}{\mathbf{l}-\mathbf{r}} \tag{40}$$

and σ an angle the value of which is given in Appendix B (see Eq. (85)-(86)). A possible approximation of σ, also derived in the appendix, is given by

$$\hat{\sigma} = 2\arctan\left(\frac{a}{b}\right)\frac{2\mathbf{m}-(\mathbf{l}+\mathbf{r})}{\mathbf{l}-\mathbf{r}} \tag{41}$$

The approximation $\hat{g}_{ts} = \hat{\varphi}^{-1}(s)$ that we have considered precisely consists in replacing in (39) σ by $\hat{\sigma}$ and $\arctan(\mathbf{m}/f)$ by $\mathbf{m}/f$. The estimate $\hat{g}$ is then calculated according to (23). Like for the previous (nonlinear) pose reconstruction method, this entails the knowledge of the sensor pose in the mobile platform and the reference position in the target frame.

Figures 9 and 10 illustrate this strategy for a fixed target and a moving target respectively. The control parameters have been defined as for the previous simulations. One can see on Fig. 9 that $\hat{g}$ provides a very good estimation of g, even for relatively large tracking errors. The resulting robot motion is very similar to the one obtained with the previous nonlinear estimation of g (compare with Fig. 7 and 8).
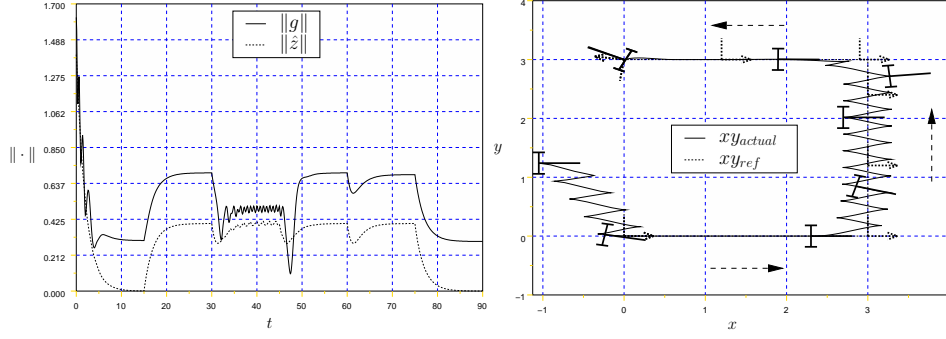
Figure 10: Nonlinear estimation of g: approximation of φ^{-1}, pan control, $\hat{c}_r = 0$

4.3.3 Generalized transverse functions

We now illustrate the possibility of using other transverse functions for the control design, in order to add flexibility in the regulation of the tracking errors. Following [9], a "generalized transverse function" is a function $f(\alpha, \beta) = (f'_g, f'_\zeta)'(\alpha, \beta)$ such that, for any (α, β), the matrix

$$\left(X(f_g(\alpha, \beta))C(f_\zeta(\alpha, \beta)) \quad \frac{\partial f_g}{\partial \alpha}(\alpha, \beta) \right)$$

is of rank three. The interest of making the transverse function depend on an extra variable β is that this variable provides extra degrees of freedom which can be used to achieve complementary objectives. Proposition 1 is easily extended to this more general framework. With $z = g f_g(\alpha, \beta)^{-1}$, we obtain, instead of (16),

$$\dot{z} = X(z)\mathrm{Ad}^X(f_g(\alpha, \beta)) \left(\bar{C}(\alpha, \beta)\bar{v} - B(\alpha, \beta)\dot{\beta} - \mathrm{Ad}^X(g^{-1})c_r(t) \right) \tag{42}$$

with $\bar{v} = (v', \dot{\alpha}')'$, $\bar{C}(\alpha, \beta) = (C(f_\zeta(\alpha, \beta)) \mid -A(\alpha, \beta))$, and $A(\alpha, \beta), B(\alpha, \beta)$ the matrices such that

$$\dot{f}_g = X(f_g(\alpha, \beta))(A(\alpha, \beta)\dot{\alpha} + B(\alpha, \beta)\dot{\beta}) \tag{43}$$

This suggests to define $\bar{v}$ as (compare with (17)–(18))

$$\bar{v} = \bar{C}(\alpha, \beta)^\dagger \left(\mathrm{Ad}^X(f_g(\alpha, \beta)^{-1})X(z)^{-1}Kz + B(\alpha, \beta)\dot{\beta} + \mathrm{Ad}^X(g^{-1})c_r(t) \right) \tag{44}$$

in order to obtain the closed-loop equation $\dot{z} = Kz$ and, subsequently, the exponential convergence of z to zero when choosing K Hurwitz-stable. In the present context, z, g, and c_r, are of course replaced in the above control expression by their respective estimates $\hat{z}$, $\hat{g}$, and $\hat{c}_r$. There remains to specify generalized transverse functions and determine a control expression for $\dot{\beta}$. Consider the function (compare with (14))

$$f_g(\alpha, \beta) = \begin{pmatrix} \varepsilon(\sin(\alpha+\beta) - \rho\sin\beta) \\ \frac{\varepsilon^2\eta}{2}((\sin(\alpha+\beta) - \rho\sin\beta)(\cos(\alpha+\beta) - \rho\cos\beta) - \rho\sin\alpha) \\ \arctan(\varepsilon\eta(\cos(\alpha+\beta) - \rho\cos\beta)) \end{pmatrix} \qquad (45)$$

It is simple to verify (see also [2]) that f_g is a generalized transverse function for the kinematic model (6) of the unicycle, for any $\varepsilon, \eta > 0$. The extra constant parameter ρ can be chosen arbitrarily. The rationale for the parameter ρ and the variable β are the following. When $\rho \in [0,1]$, one has $\max_{(\alpha,\beta)} \|f_g(\alpha,\beta)\| \leqslant 2\|(\varepsilon, \varepsilon^2\eta, \varepsilon\eta)\|$ and $\max_\beta \|f_g(0,\beta)\| \leqslant (1-\rho)\|(\varepsilon, \varepsilon^2\eta/4, \varepsilon\eta)\|$. The first inequality points out that, independently of ρ, the upperbound of $\|f_g(\alpha)\|$ can be adjusted via the choice of the parameters ε and η. The second inequality indicates that, when choosing ρ close or equal to one then, by making α tend to zero, one can keep the size of f_g small whatever the values of β and the choice made for ε and η. This suggests to use $\dot{\beta}$ as a control variable to make α tend to zero when the reference frame is motionless or when its motion is feasible for the mobile platform, in order to reduce the tracking error in these cases. On the other hand, when the motion of the reference frame is not feasible, α should be allowed to grow in order to reduce the tracking precision and, subsequently, the number of manœuvres. The following expression has been proposed in [2]:

$$\dot{\beta} = \frac{1}{1 + \rho^2 - 2\rho\cos\alpha} \left(k_t \tan(\frac{\alpha}{2}) + \frac{2}{\varepsilon\eta}(\tan(f_3)(c_{r,3}f_2 - c_{r,1}) + c_{r,3}f_1) \right) \qquad (46)$$

with $k_t > 0$, $\rho \in [0,1)$, and $c_{r,i}$ denoting the i-th component of c_r.

The simulation results reported on Fig. 11 for the tracking of a moving target illustrates this control strategy. The reference velocity c_r is chosen as in (35). The control law is given by (44) with $K = -0.5I_3$. It is assumed that the reference velocity c_r is known (either via estimation or measurement), and z, g are replaced by their estimated values $\hat{z}, \hat{g}$, with $\hat{g}$ the linear estimation of g given by Eq. (21) (as for the simulations of Fig. 4 and 5). The control of the camera pan angle is defined by (34) with $k_s = 1$. The generalized transverse function (45) is used with $\varepsilon = 0.3$, $\eta = 1$, and $\rho = 0.8$. The auxiliary control $\dot{\beta}$ is defined by (46) with $k_t = 1$. To illustrate the improvement in tracking precision which can result from using a "generalized" transverse function, we have included in Fig. 11 (top) the simulation corresponding to the "simple" transverse function (14) (with $\varepsilon = 0.3$ and $\eta = 1$). As anticipated, one can observe on Fig. 11 that the tracking error obtained with the generalized transverse function is very small during the phases when the reference trajectory is feasible (i.e. $t \in [0,30) \bigcup [45, 90]$), and that it grows otherwise (i.e. $t \in [30, 45)$), so that the manœuvres are performed at a low frequency. One can also remark that the knowledge of the target's velocity c_r improves the tracking precision significantly, and suppresses the oscillation phenomenon for backward motions of the target (compare Fig. 5 and the top of Fig. 11).
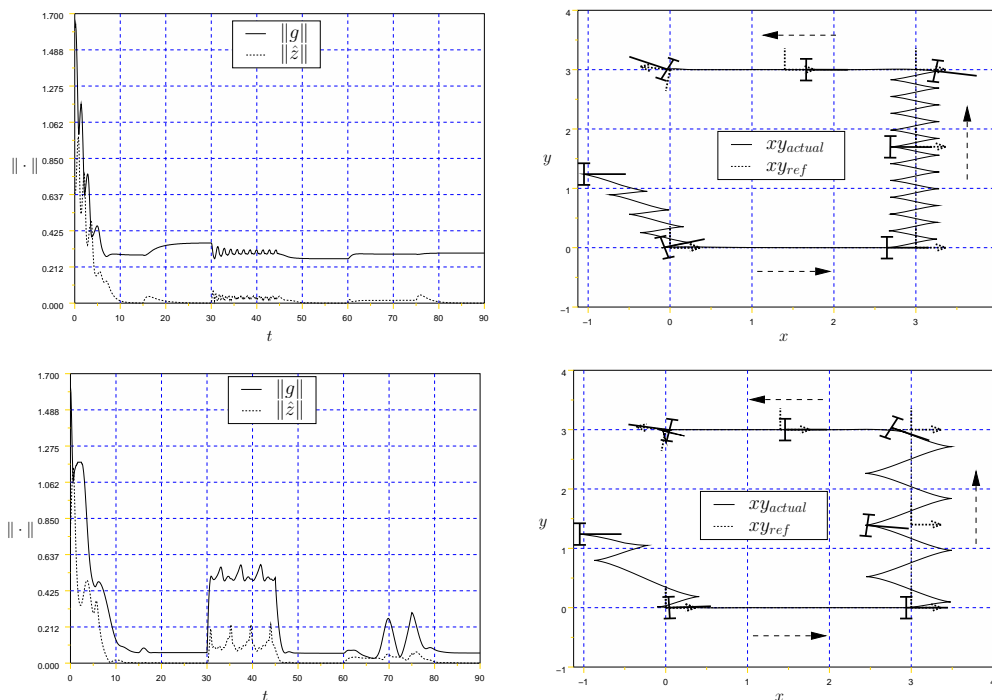
Figure 11: Linear estimation of g, pan control of the camera, simple (top) vs generalized (bottom) transverse function

4.4 Experimental results

Some experiments have been carried out with ANIS: a unicycle type mobile platform carrying a 6-DOF manipulator arm with a video camera mounted at its extremity. More details on the robot's architecture can be found on [14]. The robotic setup is the same as the one described by Fig. 2 and the geometric parameters which specify the tracking task are also those considered in the simulations, i.e. $g_{tr} = (2.5, 0, 0)'$, $g_{ms} = (0.51, 0, \xi)'$, and $a = b = 0.25$. Since we do not have sensors measuring the target's situation w.r.t. an inertial frame, only experiments with a fixed target are reported here.

The linear estimation $\hat{g}$ given by (21) is used in the control law, with the Jacobian matrices $(\frac{\partial \varphi_s}{\partial g}(0,0), \frac{\partial \varphi_s}{\partial \xi}(0,0))$ being estimated via the procedure described in Section 4.3.1, and the displacements $\Delta g(p)$ measured by odometry. The components of the signal vector s are given in pixels. A low-pass filter has been applied to the visual data in order to reduce the measurement noise.

Experiment with a simple transverse function The control law for the unicycle is given by (25) with $K = -0.5I_3$, and f defined by (14) with $\eta = 1$ and $\varepsilon = 0.3$. The control for the camera pan angle is given by (34) with $1/k_s = -\widehat{\frac{\partial \varphi_{s,2}}{\partial \xi}}(0,0)$. The motion of the robot in the Cartesian plane is shown on Fig. 12 (right). The "pseudo-true" data corresponds to a calculation of g based on the geometric reconstruction of g_{ts} given in the appendix (see Eq. (39)). This data, purposefully not used in the control law in order to test its robustness w.r.t. large pose estimation errors, provides a more accurate estimation of the actual robot's pose.
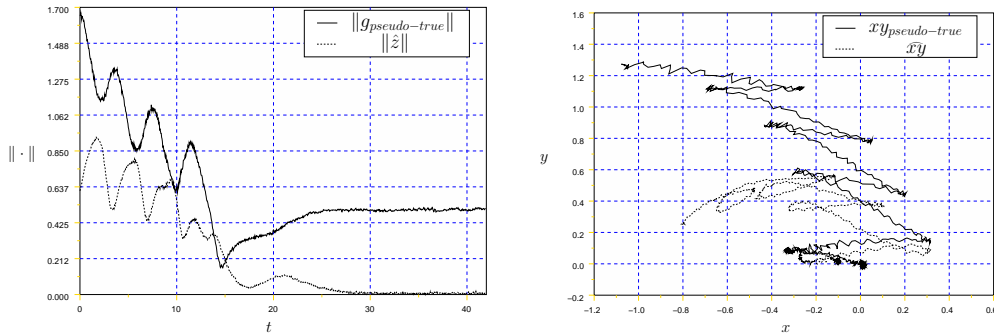

Figure 12: Experimental results with a "simple" transverse function

Experiment with a generalized transverse function The control law for the unicycle is given by (44) with $K = -0.5I_3$, and the generalized transverse function f_g is given by

(45) with $\varepsilon = 0.3$, $\eta = 1$, $\rho = 0.8$, and $\dot{\beta}$ given by (46) with $k_t = 1$. The control for the camera pan angle is the same as for the previous experiment.
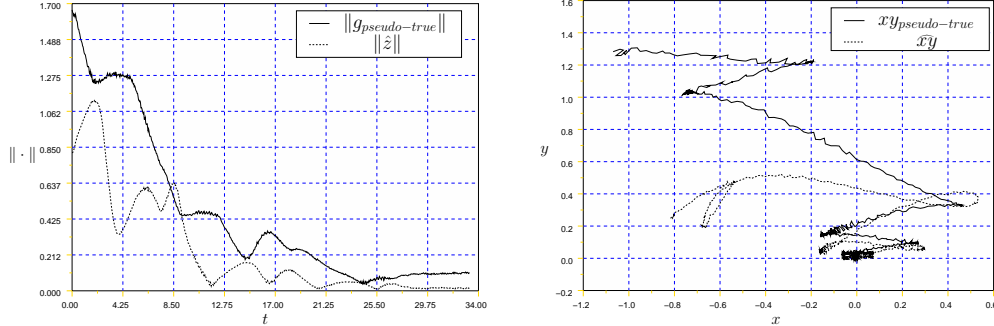

Figure 13: Experimental results with a generalized transverse function

5 Control in the space of sensor signals

We now investigate the possibility of designing stabilizing feedback laws directly in the space of sensor signals, i.e., without the intermediary calculation of an estimate of the platform's situation g. To this purpose, a first step consists in showing that the control design recalled in Section 3.3 can also be carried out in the signal space. This adaptation relies on the fact that the differential geometry properties associated with Lie groups are intrinsic, and thus independent of any choice of coordinates.

5.1 Design of practical stabilizers

Throughout this section, we assume that the signal s only depends on the relative situation g of the mobile platform w.r.t. the target, as in the case of a sensor rigidly attached to the platform, so that Eq. (20) can be written as $s = \varphi_s(g)$. The case of a relative motion between the sensor and the mobile platform will be considered further on, via an application example. Let us recall that, by assumption, φ and thus φ_s are diffeomorphisms.

Lemma 1 *In the coordinates $s = \varphi_s(g)$,*

1. *The system* (3) *is given by*[3]

$$\dot{s} = Y(s)C(\zeta)v \tag{47}$$

  with

$$Y(s) := \frac{\partial \varphi_s}{\partial g}(\varphi_s^{-1}(s))X(\varphi_s^{-1}(s)) \tag{48}$$

---

[3]To be consistent with the notation, one must set in (3) $g_{om} = g_{rm} = g$.

This system is left-invariant w.r.t. the group operation $\circ$ on $\mathbb{R}^3$ defined by $s_1 \circ s_2 = \varphi_s(\varphi_s^{-1}(s_1)\varphi_s^{-1}(s_2))$.

2. *The system (11) is given by*

$$\dot{s} = Y(s)\left(C(\zeta)v - \text{Ad}^Y(s^{-1})c_r(t)\right) \tag{49}$$

with $\text{Ad}^Y(s)$ the matrix associated with the adjoint operator, and such that

$$\forall s, \qquad \text{Ad}^Y(s) = \text{Ad}^X(\varphi_s^{-1}(s)) \tag{50}$$

3. *If $f = (f_g', f_\zeta')'$ is a transverse function for System (3), then $f_s := (f_{sg}', f_\zeta')'$, with $f_{sg} := \varphi_s(f_g)$, is a transverse function for System (47).*

The proof involves elementary calculations which are not reproduced here.

In view of this lemma, it is not difficult to extend Proposition 6 to signal coordinates.

Proposition 6 *Let $f = (f_g', f_\zeta')'$ denote a transverse function for System (3), let $\zeta = f_\zeta(\alpha)$, and define*

$$\begin{aligned} z_s &:= s \circ f_{sg}(\alpha)^{-1} \quad \text{with } f_{sg} = \varphi_s(f_g) \\ &= \varphi_s(\varphi_s^{-1}(s)f_g(\alpha)^{-1}) \end{aligned} \tag{51}$$

Then,

i) *Along the solutions of the tracking error model (49), and for any smooth curve $\alpha(.)$,*

$$\dot{z}_s = Y(z_s)\text{Ad}^X(f_g(\alpha))\left(\bar{C}(\alpha)\bar{v} - \text{Ad}^Y(s^{-1})c_r(t)\right) \tag{52}$$

with $\bar{v} = (v', \dot{\alpha}')'$ and $\bar{C}(\alpha)$ defined by (13).

ii) *The matrix $\bar{C}(\alpha)$ being of rank three for any α, the change of variable*

$$\bar{v} = \bar{C}(\alpha)^\dagger \left(\text{Ad}^X(f_g(\alpha)^{-1})v_{z_s} + \text{Ad}^Y(s^{-1})c_r(t)\right) \tag{53}$$

with $\bar{C}(\alpha)^\dagger$ a right-inverse of $\bar{C}(\alpha)$, transforms System (52) into $\dot{z}_s = Y(z_s)v_{z_s}$.

iii) *For any Hurwitz-stable matrix K, and for v_{z_s} defined by*

$$v_{z_s} = Y(z_s)^{-1}Kz_s \tag{54}$$

a) *$\|s\|$ is ultimately bounded by $\varepsilon_{f_s} := \max_\alpha \|f_{sg}(\alpha)\|$, and $\|g\|$ is ultimately bounded by $\varepsilon_f := \max_\alpha \|f_g(\alpha)\|$ for any reference trajectory $g_r(.)$,*

b) *if $c_r = 0$, s (and thus g and g_{om}) converge to fixed points exponentially.*

The proof of this proposition follows the same lines as the proof of Proposition 1 (note that the relation (50) in Lemma 1 is also used to establish (52)).

In order to calculate the feedback law (53)–(54), z_s, $Y(z_s)$ and $\mathrm{Ad}^Y(s^{-1})$ have to be known or estimated. From Lemma 1, this in turn requires to estimate the functions φ_s, φ_s^{-1}, and $\frac{\partial \varphi_s}{\partial g}$. Given such estimates (see the next section for illustrating examples), one can derive approximations $\hat{z}_s$, $\widehat{Y(z_s)}$, and $\widehat{\mathrm{Ad}^Y(s^{-1})}$ of z_s, $Y(z_s)$, and $\mathrm{Ad}^Y(s^{-1})$ respectively, simply by replacing φ_s, φ_s^{-1}, and $\frac{\partial \varphi_s}{\partial g}$ in (48), (50), and (51), by their respective estimates $\hat{\varphi}_s$, $\widehat{\varphi_s^{-1}}$, and $\widehat{\frac{\partial \varphi_s}{\partial g}}$. The control law $\bar{v}$ is then given by

$$\bar{v} = \bar{C}(\alpha)^\dagger \left(\mathrm{Ad}^X(f_g(\alpha)^{-1}) \widehat{Y(z_s)}^{-1} K \hat{z}_s + \widehat{\mathrm{Ad}^Y(s^{-1})} \hat{c}_r(t) \right) \tag{55}$$

with $\hat{c}_r(t)$ an estimation of $c_r(t)$ which, as in Section 4, may simply be set equal to zero.

5.2   Examples of estimates for z_s, $Y(z_s)$, and $\mathrm{Ad}^Y(s^{-1})$

In a way similar to the problem of pose estimation, we consider two types of estimates based either on linear, or on nonlinear, approximations of the functions φ_s, φ_s^{-1}, and $\frac{\partial \varphi_s}{\partial g}$.

Estimates based on linear approximations: A simple choice consists in using the following linear approximations:

$$\hat{\varphi}_s(g) = \widehat{\frac{\partial \varphi_s}{\partial g}}(0)g, \quad \widehat{\varphi_s^{-1}}(s) = \left(\widehat{\frac{\partial \varphi_s}{\partial g}}(0) \right)^{-1} s, \quad \widehat{\frac{\partial \varphi_s}{\partial g}}(g) = \widehat{\frac{\partial \varphi_s}{\partial g}}(0)$$

with $\widehat{\frac{\partial \varphi_s}{\partial g}}(0)$ an estimate of the jacobian matrix $\frac{\partial \varphi_s}{\partial g}(0)$. Then, by using these approximations in (48), (50), and (51), one obtains the following estimates for z_s, $Y(z_s)$, and $\mathrm{Ad}^Y(s^{-1})$:

$$\begin{cases} \hat{z}_s & = & s - \widehat{\frac{\partial \varphi_s}{\partial g}}(0) X(\hat{\theta}_s - \theta_{f_g}) f_g \\ \widehat{Y(z_s)} & = & \widehat{\frac{\partial \varphi_s}{\partial g}}(0) X \left(\left(\widehat{\frac{\partial \varphi_s}{\partial g}}(0) \right)^{-1} \hat{z}_s \right) \\ \widehat{\mathrm{Ad}^Y(s^{-1})} & = & \mathrm{Ad}^X \left(\left((\widehat{\frac{\partial \varphi_s}{\partial g}}(0))^{-1} s \right)^{-1} \right) \end{cases} \tag{56}$$

with $\hat{\theta}_s$ the third component of $(\widehat{\frac{\partial \varphi_s}{\partial g}}(0))^{-1} s$ and θ_{f_g} the third component of f_g. The above expressions can be further simplified as follows:

$$\begin{cases} \hat{z}_s & = & s - \widehat{\frac{\partial \varphi_s}{\partial g}}(0) f_g \\ \widehat{Y(z_s)} & = & \widehat{\frac{\partial \varphi_s}{\partial g}}(0) X(0) = \widehat{\frac{\partial \varphi_s}{\partial g}}(0) \\ \widehat{\mathrm{Ad}^Y(s^{-1})} & = & \mathrm{Ad}^X(f_g(\alpha)^{-1}) \end{cases} \tag{57}$$

and one can verify that $\hat{z}_s$ then corresponds to the first order approximation of z_s viewed as a function of the variables s and f_g (see (51)), that $\widehat{Y(z_s)}$ is the zero order approximation of $Y(z_s)$ at $z_s = 0$, and that $\widehat{\mathrm{Ad}^Y(s^{-1})}$ is the zero order approximation of $\mathrm{Ad}^Y(s^{-1}) = \mathrm{Ad}^Y(f_{sg}(\alpha)^{-1}z_s^{-1})$ at $z_s = 0$.

Estimates based on nonlinear approximations: When analytical expressions for $\widehat{\varphi}_s$ and $\widehat{\varphi_s^{-1}}$ are available, one can derive an analytical expression of $\frac{\partial \widehat{\varphi}_s}{\partial g}$, and use (48), (50), and (51), to form the following estimates:

$$\begin{cases} \hat{z}_s & = & \widehat{\varphi}_s(\widehat{\varphi_s^{-1}}(s)f_g^{-1}) \\ \widehat{Y(z_s)} & = & \frac{\partial \widehat{\varphi}_s}{\partial g}(\widehat{\varphi_s^{-1}}(\hat{z}_s))X(\widehat{\varphi_s^{-1}}(\hat{z}_s)) \\ \widehat{\mathrm{Ad}^Y(s^{-1})} & = & \mathrm{Ad}^X\left(\left(\widehat{\varphi_s^{-1}}(s)\right)^{-1}\right) \end{cases} \tag{58}$$

A slightly simpler expression of $\hat{z}_s$ is obtained by using the fact that, for any Lie group operation and system of coordinates such that the identity element of the group is associated with the nul vector, one has in the neighborhood of the origin $xy = x + y+$ higher order terms. This yields $z_s = s \circ f_{sg}(\alpha)^{-1} \approx s - \varphi_s(f_g)$ and the estimate $\hat{z}_s = s - \hat{\varphi}_s(f_g)$. Replacing ths first equality in (58) by this latter relation gives:

$$\begin{cases} \hat{z}_s & = & s - \widehat{\varphi}_s(f_g) \\ \widehat{Y(z_s)} & = & \frac{\partial \widehat{\varphi}_s}{\partial g}(\widehat{\varphi_s^{-1}}(\hat{z}_s))X(\widehat{\varphi_s^{-1}}(\hat{z}_s)) \\ \widehat{\mathrm{Ad}^Y(s^{-1})} & = & \mathrm{Ad}^X\left(\left(\widehat{\varphi_s^{-1}}(s)\right)^{-1}\right) \end{cases} \tag{59}$$

If an analytical expression of $\widehat{\varphi_s^{-1}}$ is available whereas an analytical expression of $\hat{\varphi}$ is not, one can define for example $\widehat{\frac{\partial \varphi_s}{\partial g}}(g) = \left(\widehat{\frac{\partial \varphi_s^{-1}}{\partial s}}(s)\right)^{-1}$, and use the linear approximation of φ_s given by $\hat{\varphi}_s(g) = \widehat{\frac{\partial \varphi_s}{\partial g}}(0)g$. Combining these relations with (48), (50), and (51), gives:

$$\begin{cases} \hat{z}_s & = & \widehat{\frac{\partial \varphi_s}{\partial g}}(0)\left(\widehat{\varphi_s^{-1}}(s)f_g^{-1}\right) \\ \widehat{Y(z_s)} & = & \left[\widehat{\frac{\partial \varphi_s^{-1}}{\partial s}}(\hat{z}_s)\right]^{-1}X(\widehat{\varphi_s^{-1}}(\hat{z}_s)) \\ \widehat{\mathrm{Ad}^Y(s^{-1})} & = & \mathrm{Ad}^X\left(\left(\widehat{\varphi_s^{-1}}(s)\right)^{-1}\right) \end{cases} \tag{60}$$

Other possible combinations are

$$
\begin{cases}
\hat{z}_s & = \quad s + \left[\widehat{\frac{\partial \varphi_s^{-1}}{\partial s}}(0) \right]^{-1} f_g^{-1} \\[2ex]
\widehat{Y(z_s)} & = \quad \left[\widehat{\frac{\partial \varphi_s^{-1}}{\partial s}}(\hat{z}_s) \right]^{-1} X(\widehat{\varphi_s^{-1}}(\hat{z}_s)) \\[2ex]
\widehat{\mathrm{Ad}^Y(s^{-1})} & = \quad \mathrm{Ad}^X\left(\left(\widehat{\varphi_s^{-1}}(s) \right)^{-1} \right)
\end{cases}
\tag{61}
$$

and

$$
\begin{cases}
\hat{z}_s & = \quad s - \left[\widehat{\frac{\partial \varphi_s^{-1}}{\partial s}}(0) \right]^{-1} f_g \\[2ex]
\widehat{Y(z_s)} & = \quad \left[\widehat{\frac{\partial \varphi_s^{-1}}{\partial s}}(\hat{z}_s) \right]^{-1} X(\widehat{\varphi_s^{-1}}(\hat{z}_s)) \\[2ex]
\widehat{\mathrm{Ad}^Y(s^{-1})} & = \quad \mathrm{Ad}^X\left(\left(\widehat{\varphi_s^{-1}}(s) \right)^{-1} \right)
\end{cases}
\tag{62}
$$

Obviously, there are many other possibilities which can be obtained, for instance, by simplifying or combining the above expressions.

5.3   Stability conditions and comparison with Section 4

To extend the stability analysis of Section 4, we would like to derive sufficient conditions on the estimates of φ_s, φ_s^{-1}, and $\frac{\partial \varphi_s}{\partial g}$ that guarantee the ultimate boundedness of s (or g), and its convergence to a fixed value when $c_r = 0$. This extension is hampered by the fact that more terms need to be estimated. Due to this first complication, stability conditions cannot, in the general case, be expressed as easily as in Section 4. Nevertheless, locally (i.e. in the neighborhood of $\hat{z}_s = 0$), one can derive boundedness and convergence conditions similar to those of Section 4.2. Moreover, and unsurprisingly, there are strong connections between the two control design methods (i.e. design in the Cartesian space versus design in the space of sensor signals). For instance, let us consider the estimates given by (56) and compare the expression of the associated control laws with the expression of some of the control laws derived in Section 4. Take the control law (24) with $\hat{g}$ given by (21). Since $\hat{z} = \hat{g} f_g(\alpha)^{-1}$, we deduce from the group law definition (1) that

$$
\begin{aligned}
\hat{z} &= \hat{g} - X(\hat{\theta}_s - \theta_{f_g}) f_g \\
&= \left(\widehat{\frac{\partial \varphi_s}{\partial g}}(0) \right)^{-1} \hat{z}_s
\end{aligned}
$$

Therefore, it follows from (56) that

$$
\hat{z}_s = \widehat{\frac{\partial \varphi_s}{\partial g}}(0) z, \ \widehat{Y(z_s)} = \widehat{\frac{\partial \varphi_s}{\partial g}}(0) X(\hat{z}), \ \widehat{\mathrm{Ad}^Y(s^{-1})} = \mathrm{Ad}^X(\hat{g}^{-1})
$$

so that the control expression (55) becomes

$$\bar{v} = \bar{C}(\alpha)^{\dagger} \left(\mathrm{Ad}^X (f_g(\alpha)^{-1}) X(\hat{z})^{-1} \bar{K}\hat{z} + \mathrm{Ad}^X(\hat{g}^{-1}) c_r(t) \right)$$

with

$$\bar{K} = \left(\widehat{\frac{\partial \varphi_s}{\partial g}}(0) \right)^{-1} K \left(\widehat{\frac{\partial \varphi_s}{\partial g}}(0) \right)$$

This is the same control as (24), except that K is replaced by $\bar{K}$. When $K = -kI_3$, the two control laws are exactly the same and thus, they share the same conditions for boundedness and convergence.

5.4 Simulation results for a vision-based sensor

To provide comparison elements between the control solutions of Sections 4 and 5, simulation results for the system of Section 4.3 (see Fig. 2), obtained with the control law defined by (55), for different choices of the estimates $\hat{z}_s$, $\widehat{Y(z_s)}$, and $\widehat{\mathrm{Ad}^Y(s^{-1})}$, are now presented.

5.4.1 Estimates based on linear approximations

When there is no pan control of the camera, and the estimates (56) are used in the control law (55) with K a diagonal matrix, we have shown above that the control expression is the same as the one obtained with the control law of Section 4 with a linear estimate of g. Therefore, we only consider here the case when the camera is actively controlled. One can imagine different ways of extending the control design of Section 5.1 to this more general setting. One of them consists in calculating from the signal and the camera pan angle ξ, the "virtual signal" s' that would be obtained if the camera were fixed to the mobile platform (i.e., with a fixed pan angle $\xi = 0$). To this purpose, let us assume, for simplicity, that the origin of the camera frame $\mathcal{F}_s = \{0_s, \vec{\imath}_s, \vec{\jmath}_s\}$ is located on the camera's pan axis (see Figure 14).

The frame associated with the "virtual camera" is denoted as $\mathcal{F}'_s = \{0_s, \vec{\imath}'_s, \vec{\jmath}'_s\}$, and the oriented angle between $\vec{\imath}'_s$ and $\vec{\imath}_s$ is ξ. A 3D point P projects into the image points p and p' in the real and virtual image planes respectively. Let γ (resp. γ') denote the oriented angle between $\vec{\imath}_s$ (resp. $\vec{\imath}'_s$) and $\overrightarrow{O_s P}$. Then, $\tan \gamma = c_1 p_y + c_2$ and $\tan \gamma' = c_1 p'_y + c_2$, with p_y and p'_y the y coordinates of the image points p, p' in the camera frames $\mathcal{F}_s$ and $\mathcal{F}'_s$, and $c_1 > 0$ and c_2 some constants depending on the camera intrinsic parameters and the unit in which p and p' are expressed (i.e. metric or pixel coordinates). From the expressions of γ and γ', the fact that $\xi + \gamma = \gamma'$, and the fact that each component s_i of the signal vector s is given by $s_i = p_{iy} - p_{iy}^*$ with $p_{iy} \in \{\mathbf{l}, \mathbf{m}, \mathbf{r}\}$, it comes that

$$s'_i = \frac{1}{c_1} \left(\tan \left(\xi + \arctan \left(c_1(s_i + p_{iy}^*) + c_2 \right) \right) - c_2 \right) - p_{iy}^* \ (i = 1, 2, 3) \tag{63}$$
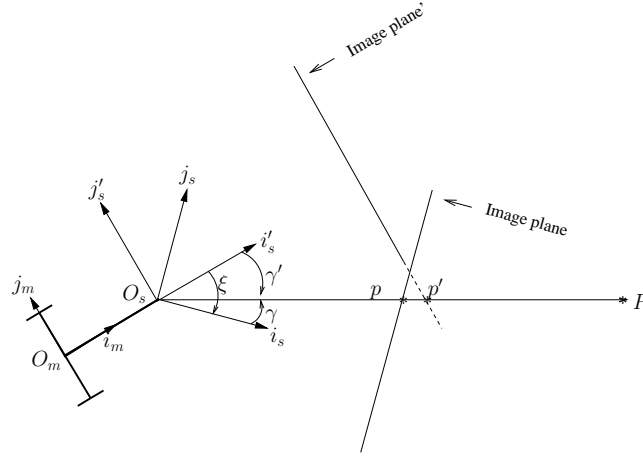
Figure 14: Projection of a 3D point in two image planes —pure rotation—

A simplification is obtained by approximating the tan and arctan functions in the above equations by the identity function. This yields

$$s' \simeq s + \frac{\xi}{c_1} \tag{64}$$

Figures 15 illustrates the use of this latter relation in the case of a fixed target. The control law is given by (55) with s in the control expression replaced by s' defined by (64) with $c_1 = 1$ (signal expressed in metric coordinates). The gain matrix is $K = -0.5I_3$ and the transverse function f_g is given by (14) with $\varepsilon = 0.3$ and $\eta = 1$. The estimates $\hat{z}_s$, $\widehat{Y(z_s)}$, and $\widehat{\mathrm{Ad}^Y(s^{-1})}$, are defined according to (57). The camera control is given by (34) with $k_s = 5$. The robot's motion is very similar to the one observed on Fig. 4 (i.e., with a control design in Cartesian coordinates and a linear pose estimation).

The same control strategy, with the same control parameters, is illustrated on Fig. 16 in the case of a moving target. The reference velocity c_r is defined by (35), and $\hat{c}_r = 0$. Unsurprisingly, the robot's motion is also very similar to the one of Fig. 5.

5.4.2 Estimates based on nonlinear approximations

We now illustrate the use of nonlinear approximations of $\hat{\varphi}_s$, $\widehat{\varphi_s^{-1}}$, and $\widehat{\frac{\partial \varphi_s}{\partial g}}$, for the calculation of the estimates $\hat{z}_s$, $\widehat{Y(z_s)}$, and $\widehat{\mathrm{Ad}^Y(s^{-1})}$. For all the simulation results reported in this section, $K = -I_3$, $\hat{c}_r = 0$, the transverse function parameters are given by $\varepsilon = 0.3$ and $\eta = 1$, the pan control of the camera is given by (34) with $k_s = 5$. The signal s', defined by (64) with $c_1 = 1$, replaces s in the control expression.
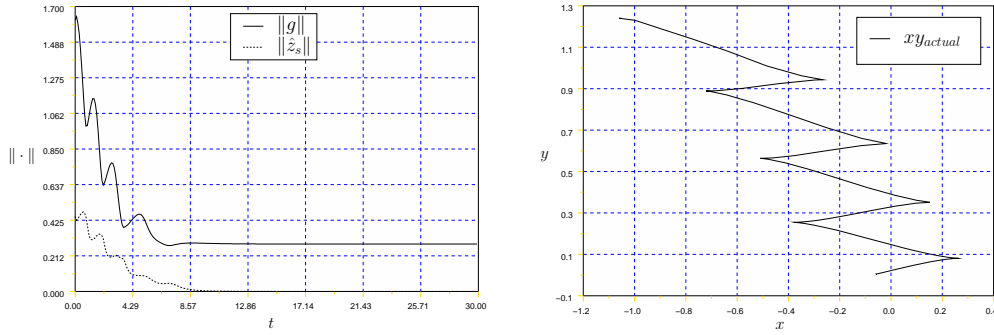
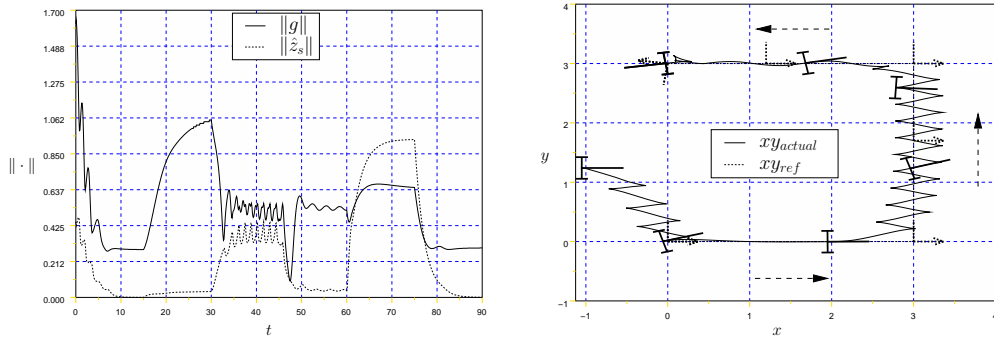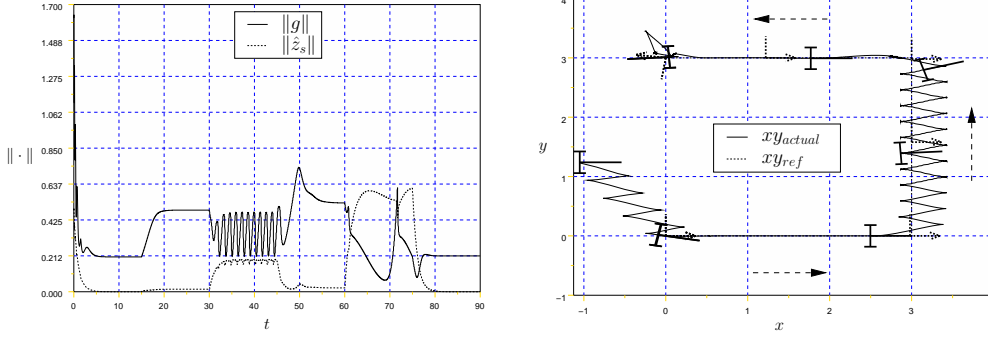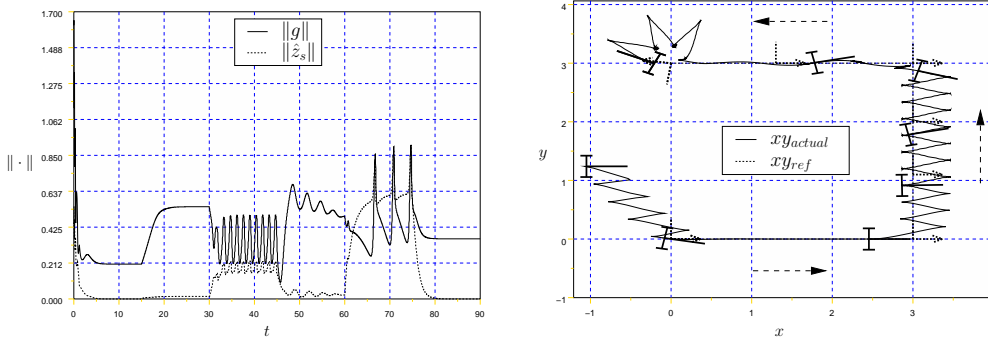Figure 15: Estimates (57), pan control of the camera, fixed target

Figure 16: Estimates (57), pan control of the camera, $\hat{c}_r = 0$

Figure 17 shows a simulation result obtained with the estimates (58). The function $\hat{\varphi}_s$ is defined from (37) and (20), i.e., $\hat{\varphi}_s(g) = \hat{\varphi}(g_{tr}gg_{ms})$ with $\hat{\varphi}$ defined by (37). The function $\widehat{\varphi_s^{-1}}$ is defined from (38), i.e. $\widehat{\varphi_s^{-1}}(s) = \hat{g} = g_{rt}\hat{g}_{ts}g_{sm}$ with $\hat{g}_{ts} = \hat{g}_{st}^{-1}$ and $\hat{g}_{st}$ given by (38).

Figure 18 shows what happens when the estimates (58) are replaced by the slightly simpler expressions (59). The robot's motion is not much different. However, one can observe a degradation of the tracking precision for purely rotational motions of the reference frame (when $t \in [60, 75]$), and the appearance of the oscillation phenomenon evoked before when the reference frame moves backward (i.e., when $t \in [45, 60]$).

Figure 19 illustrates the use of the estimates (61), with the function $\widehat{\varphi_s^{-1}}$ derived according to (39)–(41) and (23). While the tracking precision is comparable to the one associated with the previous simulations, the oscillation phenomenon for backward motions of the target is amplified. Moreover, some oscillations also occur now when the target moves forward.
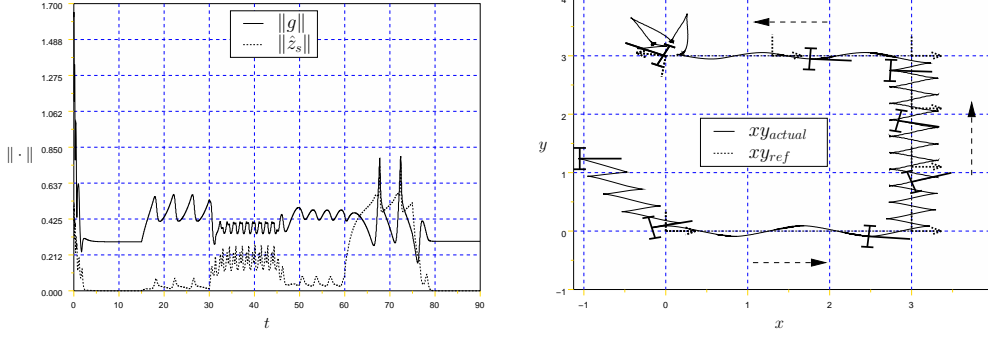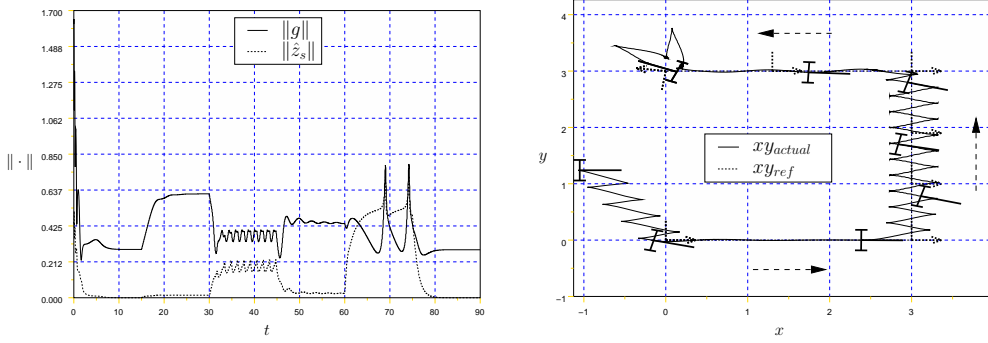
Figure 17: Estimates (58), pan-control of the camera, $\hat{c}_r = 0$

Figure 18: Estimates (59), pan-control of the camera, $\hat{c}_r = 0$

Finally, **Figure 20** illustrates the use of the estimates (62) (where only the definition of $\hat{z}_s$ changes w.r.t. the previous simulation), with the function $\widehat{\varphi_s^{-1}}$ again derived according to (39)–(41) and (23). One can note how this single modification suffices to reduce the oscillation phenomenon significantly.

5.4.3 Generalized transverse function

The extension of the control design of Section 5.1 to the use of generalized transverse functions $f(\alpha, \beta) = (f'_g(\alpha, \beta), f'_\zeta(\alpha, \beta))'$ such as (45) is straightforward. By setting $z_s = s \circ f_{sg}(\alpha, \beta)^{-1}$ with $f_{sg} = \varphi_s(f_g)$, one obtains (compare with (42) and (52)):

$$\dot{z}_s = Y(z_s)\mathrm{Ad}^X(f_g(\alpha)) \left(\bar{C}(\alpha, \beta)\bar{v} - B(\alpha, \beta)\dot{\beta} - \mathrm{Ad}^Y(s^{-1})c_r(t) \right)$$

Figure 19: Estimates (61), pan-control of the camera, $\hat{c}_r = 0$

Figure 20: Estimates (62), pan-control of the camera, $\hat{c}_r = 0$

This suggests a control law in the following form (compare with (53)–(54)):

$$\bar{v} = \bar{C}(\alpha)^{\dagger} \left(\mathrm{Ad}^X (f_g(\alpha)^{-1}) \widehat{Y(z_s)}^{-1} K \hat{z}_s + B_s(\alpha, \beta) \dot{\beta} + \widehat{\mathrm{Ad}^Y (s^{-1})} \hat{c}_r(t) \right) \tag{65}$$

with K a stable matrix and $\hat{z}_s$, $\widehat{Y(z_s)}$, and $\widehat{\mathrm{Ad}^Y (s^{-1})}$, some estimates of z_s, $Y(z_s)$, and $\mathrm{Ad}^Y (s^{-1})$, defined for example as in Section 5.2.

Figure 21 illustrates this design choice. The control law is given by (65) with $K = -0.5 I_3$. The estimates $\hat{z}_s$, $\widehat{Y(z_s)}$, and $\widehat{\mathrm{Ad}^Y (s^{-1})}$, are defined by (57), and $\dot{\beta}$ is given by (46) with $\hat{c}_r = c_r$ defined by (35) and $k_t = 1$. The generalized transverse function is defined by (45) with $\epsilon = 0.3$, $\eta = 1$, and $\rho = 0.8$. The pan control of the camera is given by (34) with $k_s = 5$. The signal s', defined by (64) with $c_1 = 1$, is used in the control law, instead of s. The robot's motion is very similar to the one shown on the bottom part of Fig. 11 (obtained

with a control design in the Cartesian space and a generalized transverse function). As a matter of fact, the tracking precision is even slightly better when the target performs purely rotational motions (time interval $[60, 75]$).
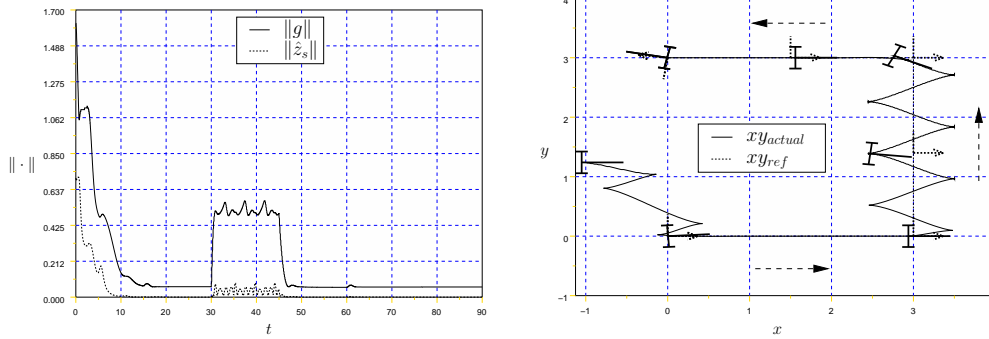

Figure 21: Generalized transverse function, pan control of the camera, $\hat{c}_r = c_r$

Conclusion

We have addressed in this report the problem of tracking, in *both position and orientation*, a moving target with a nonholonomic mobile robot, based on sensory measurements. Two control design approaches have been investigated. The first one consists in reconstructing, from the sensory data, the robot's Cartesian pose w.r.t. the target, and using this reconstruction in control laws devised for stabilization in the Cartesian space. The transverse function approach has been used for the control design and we have shown (theoretically and through various simulation results) that a stable practical tracking of the target can still be obtained when using a relatively crude model of the sensor's response (like, for example, an approximate jacobian of the sensor's output function evaluated at the reference position). This illustrates the robustness of this type of control w.r.t. modeling errors. With the example of a visual sensor (camera), we have compared different ways of reconstructing the robot's pose. While this study has confirmed the usefulness of a precise global model of the sensor, when such a model is available, it has also pointed out that good results can still be obtained with a simplified model and adequately chosen control parameters, and by compensating for the target's velocity via its estimation. The second approach consists in designing the control laws directly in the space of the sensor signals. We have shown how the transverse function approach can be extended to this sensor-based framework. The calculation of the associated control laws requires the estimation of several functions which can be expressed in terms of the sensor's output function. Simulation results do not demonstrate a definite advantage of one control design approach w.r.t. the other.

References

[1] G. Artus, P. Morin, and C. Samson. Tracking of an omnidirectional target with a nonholonomic mobile robot. In *IEEE Conf. on Advanced Robotics (ICAR)*, pages 1468–1473, 2003.

[2] G. Artus, P. Morin, and C. Samson. Control of a maneuvering mobile robot by transverse functions. In *Symp. on Advances in Robot Kinematics (ARK)*, pages 459–468, 2004.

[3] R.W. Brockett. Asymptotic stability and feedback stabilization. In R.W. Brockett, R.S. Millman, and H.J. Sussmann, editors, *Differential Geometric Control Theory*. Birkauser, 1983.

[4] A.K. Das, R. Fierro, V. Kumar, B. Southall, J. Spletzer, and C.J. Taylor. Real-time vision-based control of a nonholonomic mobile robot. In *IEEE Conf. on Robotics and Automation (ICRA)*, 2001.

[5] B. Espiau, F. Chaumette, and P. Rives. A new approach to visual servoing in robotics. *IEEE Trans. on Robotics and Automation*, 8:313–326, 1992.

[6] S. Hutchinson, G.D. Hager, and P.I. Corke. A tutorial on visual servo control. *IEEE Trans. on Robotics and Automation*, 12:651–669, 1996.

[7] D.A. Lizárraga. Obstructions to the existence of universal stabilizers for smooth control systems. *Mathematics of Control, Signals, and Systems*, 16:255–277, 2004.

[8] P. Morin and C. Samson. Practical stabilization of driftless systems on Lie groups: the transverse function approach. *IEEE Trans. on Automatic Control*, 48:1496–1508, 2003.

[9] P. Morin and C. Samson. Practical and asymptotic stabilization of chained systems by the transverse function control approach. *SIAM Journal on Control and Optimization*, 43(1):32–57, 2004.

[10] P. Morin and C. Samson. Trajectory tracking for non-holonomic vehicles: overview and case study. In K. Kozlowski, editor, *4th Inter. Workshop on Robot Motion Control (RoMoCo)*, pages 139–153, 2004.

[11] R. Pissard-Gibollet and P. Rives. Aplying visual servoing techniques to control a mobile hand-eye system. In *IEEE Conf. on Robotics and Automation (ICRA)*, pages 166–171, 1995.

[12] C. Samson, M. Leborgne, and B. Espiau. *Robot Control: The Task-function Approach*. Number 22 in Oxford Engineering. Oxford University Press, 1991.

[13] Y. Shirai and H. Inoue. Guiding a robot by visual feedback in assembling tasks. *Pattern Recognition*, 5:99–108, 1973.

[14] D. Tsakiris, K. Kapellos, C. Samson, P. Rives, and J.-J. Borelly. Experiments in real-time vision-based point stabilization of a nonholonomic mobile manipulator. In A. Casals and A. de Almeida, editors, *Experimental Robotics V: The Fifth Int. Symp.* Springer-Verlag, 1998.

A   Proofs

A.1   Proof of Proposition 2

We deduce from (16) and (25) that

$$\dot{z} = X(z)X(\hat{z})^{-1}K\hat{z} - X(z)\mathrm{Ad}^X(f)\mathrm{Ad}^X(g^{-1})c_r$$

By using the fact that, for any g_1, g_2, $\mathrm{Ad}^X(g_1)\mathrm{Ad}^X(g_2) = \mathrm{Ad}^X(g_1 g_2)$, $X(g_1)X(g_2) = X(g_1 g_2)$, and $X(g_1)^{-1} = X(g_1^{-1})$, we obtain that

$$\begin{aligned}
\dot{z} &= X(z\hat{z}^{-1})K\hat{z} - X(z)\mathrm{Ad}^X(z^{-1})c_r \\
&= X(\tilde{g})K\hat{z} - X(z)\mathrm{Ad}^X(z^{-1})c_r
\end{aligned} \tag{66}$$

We deduce from (10) that

$$X(z)\mathrm{Ad}^X(z^{-1})c_r = \begin{pmatrix} I_2 & Sp_z \\ 0 & 1 \end{pmatrix} c_r \tag{67}$$

with

$$S = \begin{pmatrix} 0 & -1 \\ 1 & 0 \end{pmatrix}$$

and p_z the position component of z (i.e. $z = (p_z', \theta_z)'$). One can also verify from (1) and (4) that

$$\hat{z} = \tilde{g}^{-1}z = \tilde{g}^{-1} + X(\tilde{g})^{-1}z \tag{68}$$

Since $K = -kI_3$, we deduce from (66), (67), and (68), that

$$\dot{z} = -kz - kX(\tilde{g})\tilde{g}^{-1} + \begin{pmatrix} I_2 & Sp_z \\ 0 & 1 \end{pmatrix} c_r \tag{69}$$

Let us now show that $g(t)$ stays in $\mathrm{B}_g(\delta_1)$, i.e. $\|g(t)\| \leqslant \delta_1$ for all t. We proceed by contradiction. Let us assume that $g(t)$ leaves $\mathrm{B}_g(\delta_1)$. Then, since $\|g(0)\| < \delta_1 - 2\varepsilon$, there exists $t_0 > 0$ such that $\|g(t_0)\| = \delta_1$ and $\|g(t)\| < \delta_1$ for all $t \in [0, t_0)$. In this interval, we deduce from (26) that

$$\begin{aligned}
\|\tilde{g}^{-1}(t)\| &= \|\tilde{g}(t)\| \\
&\leqslant \gamma_1 \|g(t)\| \\
&\leqslant \gamma_1(\|z\| + \|f\|) \\
&\leqslant \gamma_1(\|z\| + \varepsilon)
\end{aligned}$$

Let $V(z) = \|z\|^2$. We deduce from the above inequality and from (69) that

$$\begin{aligned}
\dot{V}(z) &\leqslant -2k\|z\|^2 + 2k\|z\|(\gamma_1\|z\| + \gamma_1\varepsilon) + 2\|z\|\|c_r\|_{\max} \\
&\leqslant -2k\|z\| \left((1 - \gamma_1)\|z\| - \gamma_1\varepsilon - \|c_r\|_{\max}/k\right) \\
&< 0, \qquad \forall \|z\| > \frac{\gamma_1\varepsilon + \|c_r\|_{\max}/k}{1 - \gamma_1}
\end{aligned} \tag{70}$$

It follows from (28) that $\delta_1 - \varepsilon > \frac{\gamma_1 \varepsilon + \|c_r\|_{\max}/k}{1-\gamma_1}$. Therefore, since $\|z(0)\| \leqslant \|g(0)\| + \varepsilon < \delta_1 - \varepsilon$, we deduce from (70) that $\|z(t)\| < \delta_1 - \varepsilon$, $\forall t \in [0, t_0]$, so that

$$\|g(t_0)\| \leqslant \|z(t_0)\| + \varepsilon < \delta_1$$

which shows the contradiction.

It follows from (70) that $\|z\|$ is ultimately bounded by $(\gamma_1 \varepsilon_f + \|c_r\|_{\max}/k)/(1-\gamma_1)$. This readily implies that $\|g\|$ is ultimately bounded by $\bar{\varepsilon}_f$, by using the inequality $\|g\| \leqslant \|z\| + \|f\| \leqslant \|z\| + \varepsilon_f$. $\blacksquare$

A.2   Proof of Propositions 4 and 5

Let us first establish the dynamic equation of $\hat{z}$. Since $\hat{g} = \psi(g)$, we deduce from (11) (with $c_r = 0$) that

$$\begin{aligned}
\dot{\hat{g}} &= \frac{\partial \psi}{\partial g}(g)\dot{g} \\
&= \frac{\partial \psi}{\partial g}(g)X(g)C(\zeta)v \\
&= X(\hat{g})\hat{C}(g, \zeta)v
\end{aligned}$$

with

$$\hat{C}(g, \zeta) = X(\hat{g})^{-1}\frac{\partial \psi}{\partial g}(g)X(g)C(\zeta)$$

Since $\hat{z} = \hat{g}f_g^{-1}(\alpha)$ and $\zeta = f_\zeta(\alpha)$, we deduce from the above equalities and from (9) that

$$\begin{aligned}
\dot{\hat{z}} &= X(\hat{z})\mathrm{Ad}^X(f_g(\alpha))\left(\hat{C}(g, f_\zeta(\alpha))v - A(\alpha)\dot{\alpha}\right) \\
&= X(\hat{z})\mathrm{Ad}^X(f_g(\alpha))\left(C(f_\zeta(\alpha))v - A(\alpha)\dot{\alpha} + (X(\hat{g})^{-1}\frac{\partial \psi}{\partial g}(g)X(g) - I_3)C(f_\zeta(\alpha))v\right) \quad (71) \\
&= X(\hat{z})\mathrm{Ad}^X(f_g(\alpha))\left(\bar{C}(\alpha)\bar{v} + (X(\hat{g})^{-1}\frac{\partial \psi}{\partial g}(g)X(g) - I_3)C(f_\zeta(\alpha))v\right)
\end{aligned}$$

Now, v can also be written as $v = P\bar{v}$ with P a projection matrix: for the unicycle,

$$P = \begin{pmatrix} 1 & 0 & 0 \\ 0 & 1 & 0 \end{pmatrix}$$

whereas $P = (1\ 0\ 0)$ for the car. Therefore, we deduce from (71) that

$$\dot{\hat{z}} = X(\hat{z})\mathrm{Ad}^X(f_g(\alpha))\left(\bar{C}(\alpha)\bar{v} + (X(\hat{g})^{-1}\frac{\partial \psi}{\partial g}(g)X(g) - I_3)C(f_\zeta(\alpha))P\bar{v}\right)$$

By applying the feedback law (25) to this equation, and by using the fact that $K = -kI_3$, we get

$$\dot{\hat{z}} = -k(I_3 - \mathcal{M}(\hat{z}, g, \hat{g}, \alpha))\hat{z} \quad (72)$$

with

$$\mathcal{M}(\hat{z}, g, \hat{g}, \alpha) =$$

$$X(\hat{z}) \text{Ad}^X(f_g(\alpha)) \left(I_3 - X(\hat{g})^{-1} \frac{\partial \psi}{\partial g}(g) X(g) \right) C(f_\zeta(\alpha)) P \bar{C}(\alpha)^\dagger \text{Ad}^X(f_g(\alpha)^{-1}) X(\hat{z})^{-1} \quad (73)$$

From (the proof of) Proposition 2, g exponentially converges to $\text{B}_\text{g}(\varepsilon/(1-\gamma_1))$. Therefore, in view of (72), a sufficient condition for the exponential convergence of $\hat{z}$ to zero is that

$$\|\mathcal{M}(\hat{z}, g, \hat{g}, \alpha)\| < 1 \qquad \forall (\hat{z}, \hat{g}, \alpha),\ \forall g \in \text{B}_\text{g}(\varepsilon/(1-\gamma_1)) \tag{74}$$

There remains to show that this property is satisfied. From (4) and (10), one deduces that for all z,

$$\|X(z)\| = \|X(z)^{-1}\| = 1, \quad \|\text{Ad}^X(z)\| \leqslant (1 + \|z\|), \text{ and } \|\text{Ad}^X(z^{-1})\| \leqslant (1 + \|z\|)$$

Therefore, it follows from the above definition of $\mathcal{M}(\hat{z}, g, \hat{g}, \alpha)$ and from the definition of ε that

$$\|\mathcal{M}(\hat{z}, g, \hat{g}, \alpha)\| \leqslant (1 + \varepsilon)^2 \left\| \left(I_3 - X(\hat{g})^{-1} \frac{\partial \psi}{\partial g}(g) X(g) \right) C(f_\zeta(\alpha)) P \bar{C}^\dagger(\alpha) \right\| \tag{75}$$

Then,

$$I_3 - X(\hat{g})^{-1} \frac{\partial \psi}{\partial g}(g) X(g) = X(\hat{g})^{-1} \left(X(\hat{g}) - \frac{\partial \psi}{\partial g}(g) X(g) \right)$$

$$= X(\hat{g})^{-1} \left(X(\hat{g}) - X(g) + (I_3 - \frac{\partial \psi}{\partial g}(g)) X(g) \right)$$

$$= X(\hat{g})^{-1} \left(X(\hat{g}) - X(g) + (I_3 - \frac{\partial \psi}{\partial g}(0)) X(g) - (\frac{\partial \psi}{\partial g}(g) - \frac{\partial \psi}{\partial g}(0)) X(g) \right)$$

It follows from this relations that

$$\left\| I_3 - X(\hat{g})^{-1} \frac{\partial \psi}{\partial g}(g) X(g) \right\| \leqslant \|X(\hat{g}) - X(g)\| + \|I_3 - \frac{\partial \psi}{\partial g}(0)\| + \|\frac{\partial \psi}{\partial g}(g) - \frac{\partial \psi}{\partial g}(0)\|$$

$$\leqslant \gamma_1 \|g\| + \gamma_1 + \gamma_2 \|g\|$$

$$\leqslant \gamma_1 + (\gamma_1 + \gamma_2) \|g\|$$

with the second inequality obtained from (26) and (29). We deduce from this inequality and from (75) that $\forall (\hat{z}, \hat{g}, \alpha)$ and $\forall g \in \text{B}_\text{g}(\varepsilon/(1-\gamma_1))$,

$$\|\mathcal{M}(\hat{z}, g, \hat{g}, \alpha)\| \leqslant (1 + \varepsilon)^2 \left(\gamma_1 + (\gamma_1 + \gamma_2) \frac{\varepsilon}{1 - \gamma_1} \right) \|C(f_\zeta(\alpha)) P \bar{C}^\dagger(\alpha)\|$$

$$\leqslant \left(\gamma_1 + (\gamma_1 + \gamma_2) \frac{\varepsilon}{1 - \gamma_1} \right) (1 + \varepsilon)^2 \|C(f_\zeta(\alpha)) P \bar{C}^\dagger(\alpha)\| \tag{76}$$

We now distinguish the unicycle and car-like cases.

Unicycle: In this case,

$$C(f_\zeta(\alpha)) = C = \begin{pmatrix} 1 & 0 \\ 0 & 0 \\ 0 & 1 \end{pmatrix}, \quad P = \begin{pmatrix} 1 & 0 & 0 \\ 0 & 1 & 0 \end{pmatrix}, \quad \bar{C} = \begin{pmatrix} 1 & 0 & -a_{11}(\alpha) \\ 0 & 0 & -a_{21}(\alpha) \\ 0 & 1 & -a_{31}(\alpha) \end{pmatrix}$$

with (cf. Proposition 1)

$$\begin{pmatrix} a_{11}(\alpha) \\ a_{21}(\alpha) \\ a_{31}(\alpha) \end{pmatrix} = A(\alpha) = X(f_g(\alpha))^{-1} \frac{\partial f_g}{\partial \alpha}(\alpha) \tag{77}$$

Therefore,

$$C(f_\zeta(\alpha))P\bar{C}^\dagger(\alpha) = CP\bar{C}(\alpha)^{-1} = \begin{pmatrix} 1 & -\frac{a_{11}}{a_{21}}(\alpha) & 0 \\ 0 & 0 & 0 \\ 0 & -\frac{a_{31}}{a_{21}}(\alpha) & 1 \end{pmatrix} \tag{78}$$

By using (14), (77), and (78), one can show that

$$\varepsilon \| CP\bar{C}(\alpha)^{-1} \| \leqslant \delta(\eta)(1 + \varepsilon^2) \qquad \forall \alpha \tag{79}$$

with $\delta(\eta)$ some value which only depends on η. We deduce from (76) and (79) that $\forall (\hat{z}, \hat{g}, \alpha)$ and $\forall g \in B_g(\varepsilon/(1 - \gamma_1))$,

$$\| \mathcal{M}(\hat{z}, g, \hat{g}, \alpha) \| \leqslant \left(\gamma_1 + (\gamma_1 + \gamma_2)\frac{\varepsilon}{1 - \gamma_1} \right) \frac{\bar{\delta}(\eta)(1 + \varepsilon^4)}{\varepsilon}$$

with $\bar{\delta}(\eta)$ another value. It follows from (14) that

$$\varepsilon \leqslant \varepsilon_f = \max_\alpha \| f_g(\alpha) \| \leqslant \delta_2(\eta)\varepsilon(1 + \varepsilon) \leqslant \delta_2(\eta)\varepsilon(1 + \varepsilon_f)$$

for some $\delta_2(\eta)$. By using these inequalities, one deduces that there exist some c_1, c_2, which only depend on η such that

$$\| \mathcal{M}(\hat{z}, g, \hat{g}, \alpha) \| \leqslant \left(\gamma_1 + (\gamma_1 + \gamma_2)\frac{\varepsilon_f}{1 - \gamma_1} \right) \left(\frac{c_1}{\varepsilon_f} + c_2 \varepsilon_f^3 \right)$$

so that (74) is satisfied if (30) is verified.

Car: The analysis, similar to the previous case, is left to the reader.

B   Geometric reconstruction of g used in Section 4.3.2

The objective of this section is to derive Eq. (39). Let us consider Fig. 22 which depicts, among other things, the sensor and target frames. The two lines passing by the points L, M
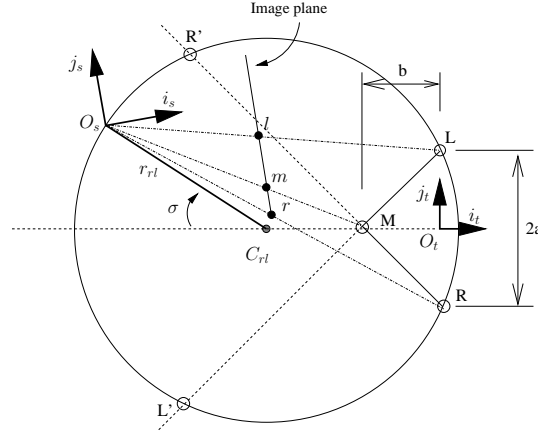
Figure 22: Camera pose reconstruction

and R, M delimit four complementary convex domains. We will assume that the origin O_s of the sensor frame is always strictly inside the convex domain opposite to the triangle LMR (as depicted on the figure). One of the reasons for this restriction is that, when O_s is on the line passing by L, M (resp. R, M), then the projections of L and M (resp. R and M) in the image plane coincide so that it is no longer possible to match each point of the target with its projection.

It is known that there is exactly one circle passing by any three non-aligned points. Let us consider the circle passing by L, O_s, and R, and denote by C_{rl} its center and r_{rl} its radius (see Fig. 22). We also denote by L' (resp. R') the points at the intersection of this circle and the line passing by L and M (resp. R and M). To provide an expression for the coordinates of O_s in the target's frame, let us define some complementary notation. We denote by α_i $(i \in \{l, m, r\})$ the oriented angles between the axis $\vec{\imath}_s$ of the sensor frame and the vector $\overrightarrow{O_s i}$. It satisfies the relation $\tan \alpha_i = \mathbf{i}/f$. The non-oriented angles $\widehat{LO_sM}$, $\widehat{LO_sR}$, and $\widehat{MO_sR}$ are denoted by α_{lm}, α_{lr}, and α_{mr} respectively. These angles satisfy the relations

$$\tan \alpha_{ij} = \frac{|\mathbf{j} - \mathbf{i}|}{|f + |\mathbf{ij}|/f|}$$

with f the focal distance.

By using the Inscribed Angle Theorem, which implies that α_{lr} is half the angle $\widehat{LC_{rl}R}$, one easily verifies that the coordinates (Cx_{rl}, Cy_{rl}) of C_{rl} in the target frame are given by

$$Cx_{rl} = -\frac{a}{\tan \alpha_{lr}}, \quad Cy_{rl} = 0 \tag{80}$$

and the radius r_{rl} of the circle is given by

$$r_{rl} = \frac{a \sqrt{(f + \frac{\mathbf{lr}}{f})^2 + (\mathbf{l} - \mathbf{r})^2}}{\mathbf{l} - \mathbf{r}} \tag{81}$$

The problem now amounts to locating the point O_s on the arc $\overset{\frown}{L'R'}$. We can parameterize this point with σ, the oriented angle between the vectors $-\vec{\imath}_t$ and $\overrightarrow{C_{rl}O_s}$. With this notation, the coordinates of O_s in the target frame are given by

$$\begin{aligned} x_{ts} &= C x_{rl} - r_{rl} \cos \sigma \\ y_{ts} &= -r_{rl} \sin \sigma \end{aligned} \tag{82}$$

There remains to calculate σ. One has

$$\begin{aligned} -r_{rl} \sin \sigma &= \sin(\alpha_{lm} + \widehat{O_s LM} - \arctan(\frac{a}{b})) \| \overrightarrow{O_s M} \| \\ &= D_{lm} \sin\left(\alpha_{lm} + \widehat{O_s LM} - \arctan(\frac{a}{b})\right) \sin \widehat{O_s LM} \end{aligned} \tag{83}$$

with

$$D_{ij} := \frac{\| \overrightarrow{IJ} \|}{\sin \alpha_{ij}} \tag{84}$$

for $i, j \in \{l, m, r\}$. Note that the law of sines has been used to obtain the second equality in (83). Note also that the D_{ij} are completely determined by the target's geometry and the angles α_{ij}. It follows from the law of sines that

$$\sin \widehat{O_s LM} = \frac{D_{mr}}{D_{lm}} \sin \widehat{O_s RM}$$

and one easily verifies on Fig. 22 that

$$\widehat{O_s RM} = 2 \arctan(\frac{a}{b}) - \alpha_{lr} - \widehat{O_s LM}$$

By combining these two equalities, one obtains that

$$\widehat{O_s LM} = \arctan\left(D_{mr} \frac{\sin(2 \arctan(\frac{a}{b}) - \alpha_{lr})}{D_{lm} + D_{mr} \cos(2 \arctan(\frac{a}{b}) - \alpha_{lr})} \right) \tag{85}$$

It follows from (83) that

$$\sigma = -\arcsin\left(\frac{D_{lm}}{r_{rl}} \left(\sin(\alpha_{lm} + \widehat{O_s LM} - \arctan(\frac{a}{b})) \sin \widehat{O_s LM} D_{lm} \right) \right) \tag{86}$$

Equations (85) and (86) provide an expression of σ in terms of the sensor signals, the focal distance, and the target's geometry. Various approximations $\hat{\sigma}$ of the above expression can be derived. Based on some very simple arguments, it is in fact possible to obtain an approximation of σ without using (86) explicitly. To this purpose, let us remark that:

- $\sigma_{max} = \max |\sigma|$ corresponds to the case where O_s coincides with L' or R'. By using the Inscribed Angle Theorem, one can verify that $\sigma_{max} = \widehat{R'LL'} = \widehat{R'RL'}$. Moreover, $\sigma_{max} = \pi - \beta - \alpha_{rl}$ with $\beta = \widehat{R'ML} = \widehat{L'MR} = \pi - 2\arctan(a/b)$. When the ratio of the distance between the target and reference frames to the target size is large, α_{rl} is small at the reference position, and tends to diminish as the distance between the robot and the target increases, thus $\sigma_{max} \simeq \pi - \beta$.

- due to the restriction assumption on the location of O_s, we have that $\alpha_{lm}, \alpha_{mr} \in [0, \alpha_{rl}]$. Furthermore, $\sigma = 0 \implies \alpha_{lm} = \alpha_{mr} = \frac{\alpha_{rl}}{2}$, $\sigma = -\sigma_{max} \implies \alpha_{mr} = 0$, and $\sigma = \sigma_{max} \implies \alpha_{lm} = 0$.

- if the camera is pointing towards the target, the angle $\alpha_m = \arctan(m/f) = 0$, so that around this position, $\alpha_m \simeq m/f$.

Based on these remarks, we propose an approximation $\hat{\sigma}$ of σ of the form $\hat{\sigma} = \rho\sigma_{max}$, with $\rho \in [-1, 1]$ such that $\alpha_{lm} = \alpha_{mr} = \frac{\alpha_{rl}}{2} \implies \rho = 0$, $\alpha_{mr} = 0 \implies \rho = 1$, and $\alpha_{lm} = 0 \implies \rho = -1$. One possibility is given by:

$$\hat{\sigma} = -\frac{\alpha_{lm} - \alpha_{mr}}{\alpha_{lr}}(\pi - \beta)$$

$$= 2\arctan(\frac{a}{b})\frac{\alpha_{mr} - \alpha_{lm}}{\alpha_{lr}}$$

Another possibility, directly expressed as a function of $\mathbf{l}, \mathbf{m}, \mathbf{r}$, is

$$\hat{\sigma} = 2\arctan(\frac{a}{b})\frac{2\mathbf{m} - (\mathbf{l} + \mathbf{r})}{\mathbf{l} - \mathbf{r}} \tag{87}$$

Finally, to complete the camera pose calculation, we need the orientation angle θ_{ts}. It is easily obtained from the coordinates of O_s and the signal values. For example,

$$\begin{aligned}
\theta_{ts} &= \arctan\left(\frac{y_{ts}}{x_{ts} + b}\right) - \alpha_m \\
&= \arctan\left(\frac{y_{ts}}{x_{ts} + b}\right) - \arctan(\frac{\mathbf{m}}{f})
\end{aligned} \tag{88}$$